The Astrophysical Journal, 789:18 (15pp), 2014 July 1 doi:10.1088/0004-637X/789/1/18

THE ENVIRONMENTAL IMPACTS ON THE STAR FORMATION MAIN SEQUENCE: AN Hα STUDY OF THE NEWLY DISCOVERED RICH CLUSTER AT $z = 1.52$

Yusei Koyama[1,2], Tadayuki Kodama[1,3], Ken-ichi Tadaki[1], Masao Hayashi[1,4], Ichi Tanaka[5], and Rhythm Shimakawa[3]
[1] National Astronomical Observatory of Japan, Mitaka, Tokyo 181-8588, Japan; koyama.yusei@nao.ac.jp
[2] Institute of Space Astronomical Science, Japan Aerospace Exploration Agency, Sagamihara, Kanagawa 252-5210, Japan
[3] Department of Astronomical Science, The Graduate University for Advanced Studies, Mitaka, Tokyo 181-8588, Japan
[4] Institute for Cosmic Ray Research, The University of Tokyo, Kashiwa, Chiba 277-8582, Japan
[5] Subaru Telescope, National Astronomical Observatory of Japan, 650 North A'ohoku Place, Hilo, HI 96720, USA
Received 2014 February 3; accepted 2014 May 13; published 2014 June 10

ABSTRACT

We report the discovery of a strong over-density of galaxies in the field of a radio galaxy at $z = 1.52$ (4C 65.22) based on our broadband and narrow-band (Hα) photometry with the Subaru Telescope. We find that Hα emitters are located in the outskirts of the density peak (cluster core) dominated by passive red-sequence galaxies. This resembles the situation in lower-redshift clusters, suggesting that the newly discovered structure is a well-evolved rich galaxy cluster at $z = 1.5$. Our data suggest that the color–density and stellar mass–density relations are already in place at $z \sim 1.5$, mostly driven by the passive red massive galaxies residing within $r_c \lesssim 200$ kpc from the cluster core. These environmental trends almost disappear when we consider only star-forming (SF) galaxies. We do not find SFR–density or SSFR–density relations amongst SF galaxies, and the location of the SF main sequence does not significantly change with environment. Nevertheless, we find a tentative hint that star-bursting galaxies (up-scattered objects from the main sequence) are preferentially located in a small group at ∼1 Mpc away from the main body of the cluster. We also argue that the scatter of the SF main sequence could be dependent on the distance to the nearest neighboring galaxy.

Key words: galaxies: active – galaxies: evolution – galaxies: clusters: general

Online-only material: color figures

1. INTRODUCTION

Recent observations have established that star-forming (SF) galaxies show a tight correlation between stellar mass ($M_\star$) and star-formation rate (SFR). This SFR–$M_\star$ correlation (the so-called SF main sequence) is investigated in the local universe (e.g., Brinchmann et al. 2004; Peng et al. 2010), as well as in the distant universe out to $z \gtrsim 2$ (e.g., Noeske et al. 2007; Daddi et al. 2007; Elbaz et al. 2007; Santini et al. 2009; Kajisawa et al. 2010; Rodighiero et al. 2010; Bauer et al. 2011a; Whitaker et al. 2012). The SFR at a fixed mass evolves with time, reflecting the cosmic star formation history. The presence of this tight SFR–$M_\star$ correlation suggests that stellar mass has always been an important parameter that regulates SF activity in galaxies across cosmic time.

The scatter around the SF main sequence is reported to be very small ($\lesssim$0.3 dex level at any redshifts), but the deviation around the SF main sequence may be an important parameter as it likely reflects the variation of gas accretion/exhaustion history of galaxies (e.g., Elbaz et al. 2011; Saintonge et al. 2012; Tacconi et al. 2013). Some recent studies attempt to identify the origin of the scatter and the key parameter that makes the strongest impact on galaxy evolution. For example, Wuyts et al. (2011) studied how the galaxy structure and the mode of SF activity depend on the position on the SFR–$M_\star$ diagram. They find that the upper envelope of the SF main sequence tends to be dominated by dusty galaxies (characterized by high $\mathrm{SFR_{IR}}/\mathrm{SFR_{UV}}$ ratio) with high Sersic index (n), suggesting a rapid build-up of mass in the nuclear regions of these systems, due to, e.g., galaxy–galaxy interactions/mergers.

Another important parameter that could bring strong impacts on SF activity of galaxies is "environment." The morphology–density or color–density relation is widely recognized in the local universe (e.g., Dressler 1980; Lewis et al. 2002; Gómez et al. 2003; Goto et al. 2003; Tanaka et al. 2004). However, if we focus on the SF population, their properties are not necessarily strong functions of environment. Balogh et al. (2004) used the Sloan Digital Sky Survey (SDSS) and 2dFGRS data sets to show the Hα equivalent width (EW) amongst SF galaxies is independent of environment (see also Wijesinghe et al. 2012). Peng et al. (2010) used local SF galaxies drawn from SDSS to show that the SF main sequence is indistinguishable between high- and low-density environments. They argue that the environment does change the "fraction" of SF galaxies, while it has very little impact on the SF main sequence.

An observational challenge here is to test if the "universality" of SF main sequence holds in the distant universe, where the average star-formation activity is about an order of magnitude higher (e.g., Madau et al. 1996). Some recent studies have attempted to identify the environmental dependence of the SF main sequence from intermediate- to high-redshift universe out to $z \sim 2$ (Vulcani et al. 2010; Li et al. 2011; McGee et al. 2011; Muzzin et al. 2012; Greene et al. 2012; Tanaka et al. 2011; Grützbauch et al. 2011; Koyama et al. 2013a; Zeimann et al. 2013; Ziparo et al. 2014), but a full consensus has not yet been obtained because of the different sample selection and/or different environment definitions. The most recent study by Lin et al. (2014) used a large sample of galaxies drawn from Pan-STARRS, and demonstrated that the (S)SFR–$M_\star$ relation for SF galaxies is comparable between field and group environment out to $z \sim 0.8$. They also reported that there is a moderate (∼17%) SFR decrease for SF galaxies (at a given mass) in cluster environment. Pushing this kind of study toward the critical epoch of galaxy formation (i.e., $z \sim$ 1–3) is clearly an important step, but constructing a large uniformly selected SF galaxy sample

across environment at such high-redshift universe has been very challenging.

Recently, Koyama et al. (2013b) made an important step toward resolving this issue. They compiled a large, Hα-selected SF galaxy sample in distant clusters (from MApping HAlpha and Lines of Oxygen with Subaru (MAHALO-Subaru) project; Kodama et al. 2013) and in general field environments at $z = 0.4, 0.8, 2.2$ (from HiZELS; Sobral et al. 2013), and demonstrated that the environmental impacts on the SF main sequence are likely always small since $z \sim 2$ (<0.2 dex level at maximum), as far as we rely on the simple Hα-based SFRs. However, in contrast to this apparently simple picture, we also find a tentative hint that SF galaxies in distant cluster environments tend to be more massive (see also Lin et al. 2014), and perhaps more highly obscured by dust. In this paper, we provide a more detailed look at this issue and attempt to identify the environmental impacts on the SF main sequence using our newly discovered rich cluster field at $z \sim 1.5$.

The paper is organized as follows. In Section 2, we present our Subaru data of the 4C 65.22 field. After selecting $z \approx 1.5$ galaxies based on our photometric data in Section 3, we report the discovery of a strong over-density of $z \sim 1.5$ galaxies near the radio galaxy in Section 4. In Section 5, we present environmental dependence of galaxy properties at $z \sim 1.5$ across the newly discovered structure. In Section 6, we discuss our results in line with recent studies. Finally, our conclusions are given in Section 7. Throughout the paper, we adopt $\Omega_M = 0.3$, $\Omega_\Lambda = 0.7$, and $H_0 = 70$ km s^{-1}Mpc^{-1}, which gives a 1″ scale of 8.46 kpc and the cosmic age of 4.2 Gyr at the redshift of our target cluster associated with the radio galaxy, 4C 65.22 ($z = 1.520$). Magnitudes are all given in the AB system.

2. OBSERVATION AND DATA REDUCTION

2.1. The Field of a Radio Galaxy 4C 65.22 ($z = 1.52$)

In this paper, we aim to present our newly discovered rich galaxy cluster at $z \sim 1.5$. An increasing number of high-z galaxy clusters are now being discovered with various techniques (e.g., Tanaka et al. 2010; Papovich et al. 2010; Fassbender et al. 2011; Gobat et al. 2011; Newman et al. 2014), but it is still very important to increase the sample of clusters/groups in the distant universe. For this purpose, high-z radio galaxies (HzRGs) are often used as "landmarks" for high-z (proto-) clusters since HzRGs are expected to be the progenitors of present-day massive cluster ellipticals (e.g., Kurk et al. 2000, 2004; Venemans et al. 2002; Best et al. 2003; Kajisawa et al. 2006; Venemans et al. 2007; Kodama et al. 2007; Galametz et al. 2010, 2013). These studies have been successful in identifying prominent high-z structures.

We have been undertaking an intensive observational program of high-z SF galaxies using narrow-band filters on the Subaru Telescope, MAHALO-Subaru (Kodama et al. 2013, Tadaki et al. 2011; Hayashi et al. 2012, 2014; Koyama et al. 2013a). As a part of this observational campaign, we target a radio galaxy field, 4C 65.22, at $z = 1.520$ ($\alpha = 17^h47^m13.^s9$, $\delta = +65°32'36''$ in J2000),[6] which is located near the North Ecliptic Pole. 4C 65.22 is identical to 8C 1747+655, and a strong X-ray detection is reported from this radio galaxy (see Brinkmann et al. 1999; Kollgaard et al. 1994; 1995; Lacy et al. 1993). Below we describe our new Subaru observations of this radio galaxy field.

[6] We exploit $z = 1.520$ as the redshift of 4C 65.22 following the [O II]-line-based measurement presented by Kollgaard et al. (1995). These authors reported slightly different redshifts for other line measurements (such as C IV, C III], or Mg II), although the difference is negligibly small for our study ($\Delta z \lesssim 0.005$ level).

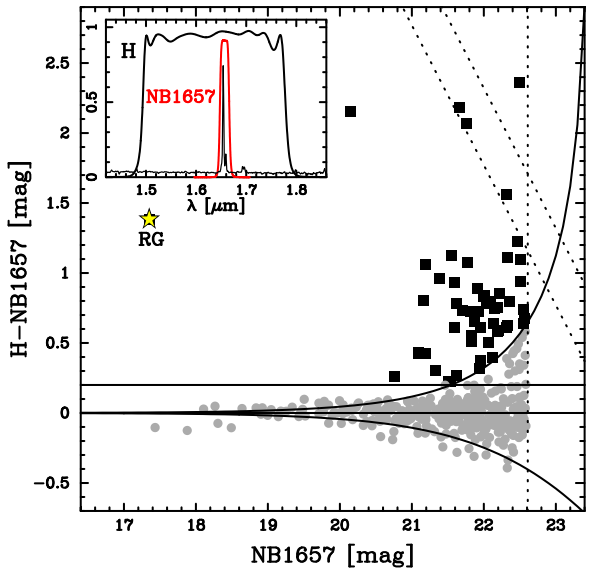

Figure 1. Selection of the NB1657 emitters. We plot $H-$NB1657 colors of all NB-selected galaxies against their NB magnitudes. The vertical dotted line shows the 5σ limiting magnitude in NB1657, and the slanted dotted lines show 2 and 3σ limits in H-band. The solid curves show $\pm 2\Sigma$ excesses in the $H-$NB1657 color. We select galaxies with $H-$NB1657 > 0.2 and with $H-$NB1657 > 2Σ as NB1657 emitters (black squares). The brightest galaxy (marked with a yellow star) is the central radio galaxy (4C 65.22), showing a strong NB excess as expected. In the inset, we show the transmission curves of the broad-band (H) and narrow-band (NB1657) filters. Also shown is the Sc-type galaxy spectrum (redshifted to $z = 1.52$) from Kinney et al. (1996).

(A color version of this figure is available in the online journal.)

2.2. Near-infrared Data with MOIRCS

We observed the 4C 65.22 field with broadband (*JHKs*) and narrow-band (NB1657) filters using the Multi-Object InfraRed Camera and Spectrograph (MOIRCS; Ichikawa et al. 2006; Suzuki et al. 2008) on the Subaru Telescope (Iye et al. 2004). The MOIRCS covers a $4' \times 7'$ field of view (FoV), which corresponds to the physical scale of 2.0×3.6 Mpc^2 at $z \sim 1.5$. We note that the NB1657 filter ($\lambda_c = 1.657\,\mu$m, $\Delta\lambda = 0.019\,\mu$m; see Figure 1) captures the Hα lines at $z = 1.52^{+0.02}_{-0.01}$ (or equivalently $-1200 \lesssim \Delta v \lesssim 2300$ km s^{-1} from the radio galaxy), and this filter plays a critical role in this study (see Section 3.1 for the Hα emitter selection). The observations were carried out in 2011 September under excellent conditions. The data were reduced using the MCSRED software (Tanaka et al. 2011) in a standard manner. For the narrowband (NB) data reduction, we use the "NBMCSALL" task provided in the MCSRED package, which is dedicated to the MOIRCS NB data reduction. This task takes a careful treatment for the variation of sky patterns over the MOIRCS FoV (see Tanaka et al. 2011 for details). The photometric zero points are derived with the standard stars observed during the same observing nights. The exposure times, point-spread function (PSF) sizes, and limiting magnitudes of our MOIRCS data are summarized in Table 1.

2.3. Optical Data with Suprime-Cam

We also use B-, r'-, and z'-band data of the 4C 65.22 field taken with the Prime Focus Camera on Subaru (Suprime-Cam; Miyazaki et al. 2002). The r'- and z'-band data are newly obtained by our team in 2010 October, while the B-band data

Table 1
Summary of Our Subaru Data of the 4C 65.22 Field

Filter	Instrument	Obs. Date (UT)	Exp Time (min)	PSF Size (arcsec)	Limit Mag. ($1\farcs5$, 5σ, AB)	$A_{\rm band}$ (mag)
B	Suprime-Cam	2005 Aug 30	108	0.95	27.4	0.19
r'	Suprime-Cam	2010 Oct 7,8	94	0.92	26.9	0.12
z'	Suprime-Cam	2010 Oct 6	42	0.62	25.3	0.06
J	MOIRCS	2011 Sep 6	87	0.60	23.9	0.04
H	MOIRCS	2011 Sep 6,7	66	0.49	23.3	0.03
K_s	MOIRCS	2011 Sep 8	48	0.60	23.2	0.02
NB1657	MOIRCS	2011 Sep 7,8	183	0.56	22.6	0.03

Note. The B-band data are retrieved from SMOKA (Subaru Science Archive: http://smoka.nao.ac.jp/).

are retrieved from Subaru Science Archive (SMOKA). All the data are reduced with SDFRED pipeline software developed for the Suprime-Cam data reduction (Yagi et al. 2002; Ouchi et al. 2004). We use SDFRED1 for the B-band data reduction, while we use SDFRED2 (minor updated version) for the reduction of r'/z' data according to the Suprime-Cam CCD upgrade in 2008. The magnitude zero points are derived from the data of standard stars taken during the same observing nights. We note that the original FoV of Suprime-Cam is $34'\times27'$, but we only use central $4'\times7'$ region in this study due to the limited FoV of our near-infrared (NIR) data. The final optical images are aligned to our MOIRCS image and re-gridded to the pixel scale same as the MOIRCS data ($0\farcs117$ pixel^{-1}).

2.4. Photometric Catalog

The photometric catalog is created with `SExtractor` version 2.5.0 (Bertin & Arnouts 1996). Before running `SExtractor`, we apply Gaussian smoothing for the NIR images, and match their PSF sizes to $0\farcs62$ (i.e., PSF of z'-band image). We note that the B- and r'-band data have broader PSF size ($0\farcs9$–$1\farcs0$; see Table 1). We apply an aperture correction of 0.165/0.145 mag for the B/r'-band data when we perform aperture photometry, rather than degrading our good-quality NIR data by ∼50%–100%. These correction values are determined by a simple simulation using our z'-band image: we smoothed the z'-band image to $0\farcs95/0\farcs92$ (i.e., the PSF size of B/r'-band image), and then performed $1\farcs5$ aperture photometry of the same sources on the smoothed/unsmoothed images to determine the typical fluxes escaped from the aperture.

The limiting magnitudes are determined by measuring the deviation of $1\farcs5$ aperture photometry (2.5×PSF size) at random positions over the FoV, and the measured limiting magnitudes are reported in Table 1. The measured 1σ random sky noise on each image is also used as the photometric uncertainties of individual sources. Following our previous high-z emission-line galaxy surveys carried out with the MAHALO project, we construct a NB-selected source catalog using the double image mode of `SExtractor`. In this study, we use $1\farcs5$ aperture magnitudes (MAG_APER) for source detection and measuring colors, while we use total magnitude (MAG_AUTO) when we derive physical quantities such as $M_\star$ or SFRs of galaxies.

Using the stellar spectral templates of Gunn & Stryker (1983), we checked colors of stellar objects within the FoV. We find that the derived zero points show good agreement with the template, but we apply a small zero point correction to H-band magnitudes by +0.1 mag to be consistent with the stellar template. After removing saturated objects and galactic stars (based on the BzK and rJK colors; see Figure 2), our final catalog includes 393 objects down to $m_{\rm NB} = 22.6$ mag (corresponding to 5σ limit in NB1657). At the position of 4C 65.22, we estimate the dust reddening to be $E(B-V) = 0.042$ mag based on the dust map of Schlegel et al. (1998). We derive the correction value at each band using the extinction law of Cardelli et al. (1989), and the derived correction values ($A_{\rm band}$) are listed in Table 1.

3. SAMPLE SELECTION

In this section, we select galaxies at $z \approx 1.5$ using our photometric catalog. The primary goal of this project is to map the Hα-emitting galaxies around 4C 65.22 with the narrow-band technique (Section 3.1). We also apply photometric redshifts (photo-z) to select a more quiescent galaxy population (Section 3.2). By combining these SF and quiescent galaxies, we construct a catalog of "member" galaxies associated with the central radio galaxy.

3.1. Hα Emitter Selection

We first select Hα emitters at $z = 1.52$ using the narrow-band excess technique. Our selection includes the following two steps: (1) identification of NB excess galaxies using $H-$NB1657 color, and (2) removal of contaminant emitters (such as [O II]/Hβ/[O III] emitters at higher redshifts, or various line-emitting galaxies at low redshifts) based on their broad-band colors.

In Figure 1, we plot the $H-$NB1657 colors of all NB-selected galaxies against their NB magnitudes. To select NB excess sources, we apply $H-$NB1657 > 0.2 and $H-$NB1657 $> 2\,\Sigma$, where Σ denotes the significance of NB excess (Bunker et al. 1995). This yields 54 galaxies with NB excess, and they are shown with the black squares in Figure 1. We note that the former condition corresponds to EW$_{\rm rest} \gtrsim 20$ Å and the latter corresponds to dust-free SFR$_{\rm H\alpha}$ of $\gtrsim 3 M_\odot$ yr^{-1} (see Section 5.2 for more details).

Next, we remove the expected contaminant galaxies, such as low-redshift Paβ emitters at $z \approx 0.3$, Hβ/[O III] emitters at $z \approx 2.3$, or [O II] emitters at $z \approx 3.3$. The presence of a strong emission line located at $\lambda \simeq 1.657\,\mu$m allows us to determine their redshifts using broadband color information (see, e.g., Kodama et al. 2004; Koyama et al. 2010). We find that most of the NB1657 emitters are detected with our deep broadband images, while we find two of the NB1657 emitters are fainter than the 2σ limit in K_s-band. The K_s-band photometry is very important in the following member selection, and it is also essential for deriving stellar mass of galaxies (see Section 5.1). We therefore exclude these two K_s-undetected objects from the following analysis.

In Figure 2 (left), we show the BzK diagram to remove low-z contamination. The BzK method is originally proposed

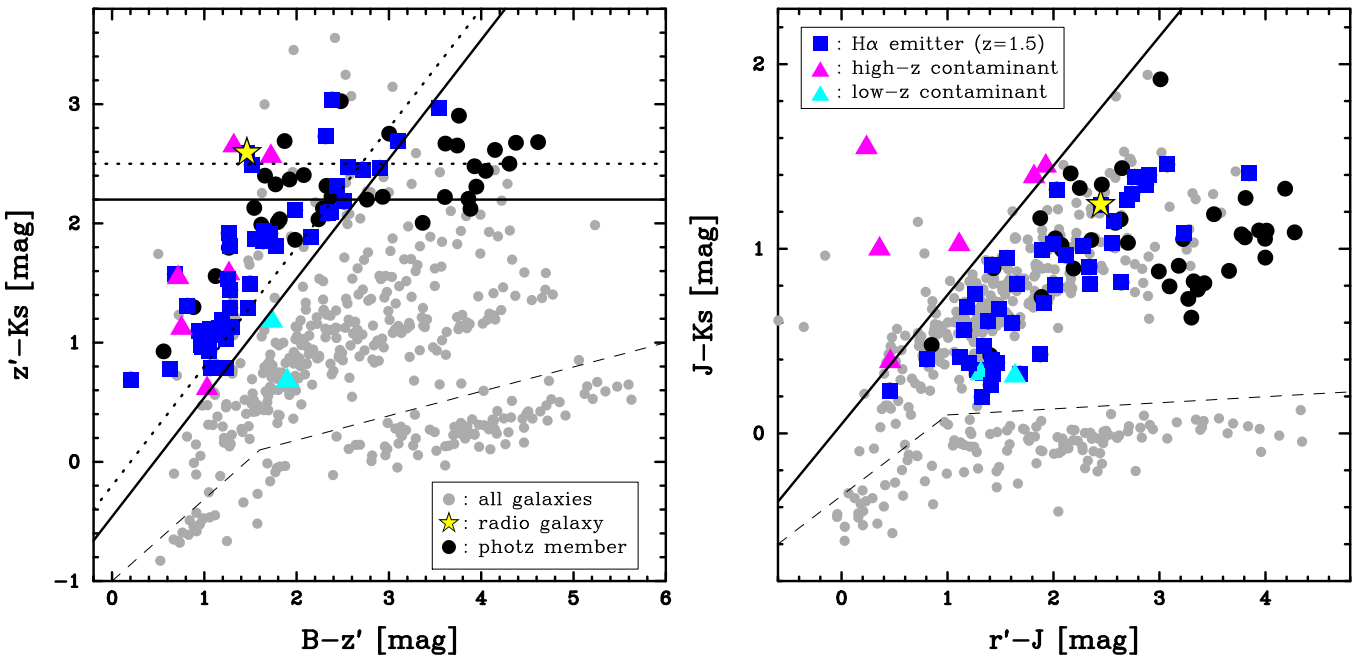

Figure 2. Color selections of Hα emitters at $z = 1.52$ based on the *BzK* (left) and *rJK* (right) color–color diagrams. We here plot all NB-selected sources with $>2\sigma$ detection at all broadband filters including galactic stars (gray dots). The NB1657 emitters selected in Figure 1 are shown with colored symbols. The *BzK* diagram isolates low-z contamination (cyan triangles), and the *rJK* diagram isolates high-z contamination such as [O III] emitters at $z = 2.31$ (magenta triangles). The Hα emitters are defined as NB1657 emitters satisfying both *BzK* and *rJK* criteria, and they are shown with blue squares. The solid lines show the criteria applied in this study. The dotted lines in the left panel show the original *BzK* criteria proposed by Daddi et al. (2004), while we apply the modified-*BzK* criteria to improve completeness for $z \sim 1.5$ galaxies (Hayashi et al. 2011). Sources below the thin dashed lines are galactic stars and discarded from our catalog. The radio galaxy (shown with a yellow star) satisfies both *BzK* and *rJK* criteria. We also plot photo-z selected non-emitters with black circles ($1.3 < z_{\rm phot} < 1.7$; see Section 3.2). As expected, most of the photo-z members satisfy both color criteria.

(A color version of this figure is available in the online journal.)

by Daddi et al. (2004), and is one of the most commonly used color selections for high-z galaxies. The *BzK* method is designed to select galaxies at $1.4 \lesssim z \lesssim 2.5$ and optimized for $z \sim 2$ galaxies. Therefore, galaxies at $z \sim 1.5$ are usually located near the border lines of the *BzK* criteria. Hayashi et al. (2010) proposed a "modified *BzK* selection" for selecting $z \sim 1.5$ galaxies, which slightly softens the criteria toward the bluer side by ∼0.2 mag (see the solid lines in Figure 2, left). The robustness of this method is demonstrated by our spectroscopic follow-up study (Hayashi et al. 2011). The colored symbols in Figure 2 show the NB1657 emitters selected above. We find that most of the emitters satisfy the *sBzK* criteria as expected, while two of the NB emitters are likely low-z contamination (shown as cyan triangles in Figure 2).

We then apply *rJK* selection to remove high-z contamination at $z > 2$ (the right panel of Figure 2). This method is proposed by Hayashi et al. (2012) to distinguish $z \gtrsim 2.5$ galaxies from $z < 2$ galaxies, and the robustness of this method is shown by our recent spectroscopic observation (Shimakawa et al. 2014). With this technique, we find that six of the NB1657 emitters are likely high-z emitters at $z > 2$ (see the magenta triangles in Figure 2), and they are now excluded from our catalog. In summary, among the 52 NB emitter candidates (with K_s-band detection), we identify a total of eight contaminant emitters (two low-z and six high-z objects). In the following analysis, we consider the remaining 44 emitters as Hα emitters at $z = 1.52$. The list of the selected Hα emitters is provided in Table 2.

3.2. Photometric Redshifts and the Final Member Catalog

We use photometric redshifts ($z_{\rm phot}$) to select non-Hα-emitting passive members (with strong 4000 Å break) which cannot be identified with the above Hα emitter selection. We here restrict the sample to those detected at $>2\sigma$ level with at least four bands out of the six broad-band images ($Br'z'JHK_s$). The best-fit photometric redshifts are computed with a simple template fitting following the standard χ^2 minimizing statistics using EAZY code (Brammer et al. 2008). The distribution of the derived $z_{\rm phot}$ is shown in Figure 3. The photometric redshifts derived with only six broadband filters may not be very accurate, but it is worth mentioning that there is a clear redshift spike at $z_{\rm phot} \sim 1.5$ near the radio galaxy (top panel of Figure 3). In the following analysis, we apply a photo-z cut of $1.3 < z_{\rm phot} < 1.7$ (dotted lines in Figure 3) to select member galaxies associated with the radio galaxy. With this criteria, we select 61 galaxies in total, among which 20 galaxies are within the central 250 kpc region.[7]

As shown in Figure 2 (black circles), most of the photo-z-selected galaxies satisfy the *BzK* and *rJK* criteria. Unfortunately, we cannot fully quantify the photo-z accuracy because no spec-z information is available in the observed field. However, we emphasize that our results do not change even if we apply simple color selections without relying on the photometric redshift. We here crudely test the contamination level by using the UKIDSS/UDS data, where *BRzJHK* data are publicly available (Lawrence et al. 2007).[8] After applying the same magnitude cuts, we derive photo-z of the UDS galaxies in the same way as described above. We find that ∼2250 galaxies (out of ∼25,000 sources) satisfy the $1.3 < z_{\rm phot} < 1.7$ criteria over the entire ∼0.8 deg^2 UDS field,

[7] We compute the density peak using all the member galaxies, including photo-z members and Hα emitters, and exploit this point as the cluster center (see also Figure 4).

[8] http://www.nottingham.ac.uk/astronomy/UDS/index.html

Table 2
List of the 44 Hα Emitters in the Field of 4C 65.22 Selected in Section 3.1

ID	R.A. (deg)	Decl. (deg)	H mag (AB, 1.″5)	NB1657 mag (AB, 1.″5)	EW_r(Hα+[N II]) (Å)	F(Hα+[N II]) (10^{-16} erg s^{-1} cm^{-2})	$\log(M_\star/M_\odot)$[a]
12	266.76831	65.57383	22.57 ± 0.10	21.96 ± 0.11	83.3 ± 6.3	1.53 ± 0.35	10.43 ± 0.06
13	266.76767	65.57382	22.96 ± 0.14	22.33 ± 0.16	11.4 ± 6.2	0.13 ± 0.25	10.41 ± 0.05
14	266.67044	65.57362	23.82 ± 0.30	21.75 ± 0.09	1069.6 ± 274.2	1.73 ± 0.24	9.82 ± 0.11
293	266.82201	65.51409	22.65 ± 0.11	21.92 ± 0.11	163.1 ± 12.8	1.42 ± 0.27	10.14 ± 0.08
357	266.76742	65.51608	22.53 ± 0.10	21.88 ± 0.10	94.1 ± 8.4	0.93 ± 0.25	10.75 ± 0.04
409	266.78674	65.51795	22.33 ± 0.08	21.95 ± 0.11	50.0 ± 5.9	0.64 ± 0.25	10.70 ± 0.03
576	266.70583	65.52318	21.89 ± 0.06	21.62 ± 0.08	21.6 ± 3.5	0.45 ± 0.24	11.06 ± 0.02
761	266.89357	65.53110	22.89 ± 0.14	22.14 ± 0.13	66.9 ± 7.7	0.77 ± 0.28	10.81 ± 0.04
858	266.64000	65.53503	21.64 ± 0.04	21.33 ± 0.07	26.0 ± 2.7	0.72 ± 0.25	11.31 ± 0.01
870	266.69924	65.53562	22.25 ± 0.08	21.94 ± 0.11	14.4 ± 3.9	0.30 ± 0.28	10.93 ± 0.03
874	266.90847	65.53584	22.39 ± 0.09	21.83 ± 0.10	55.0 ± 5.3	0.91 ± 0.28	10.63 ± 0.03
930	266.79381	65.53762	22.77 ± 0.12	22.19 ± 0.14	41.8 ± 6.9	0.47 ± 0.26	10.32 ± 0.06
1002	266.68019	65.54095	22.40 ± 0.09	21.62 ± 0.08	83.6 ± 6.2	1.11 ± 0.25	10.73 ± 0.03
1006	266.82164	65.54123	22.92 ± 0.14	22.31 ± 0.15	70.6 ± 10.7	0.49 ± 0.23	10.45 ± 0.06
1043[b]	266.80809	65.54326	18.73 ± 0.00	17.35 ± 0.00	298.4 ± 0.5	108.00 ± 0.28	12.33 ± 0.00
1046	266.81166	65.54294	21.73 ± 0.05	21.51 ± 0.08	20.7 ± 2.6	0.72 ± 0.30	11.38 ± 0.01
1085	266.77394	65.54452	22.84 ± 0.13	22.00 ± 0.12	192.7 ± 16.4	1.49 ± 0.29	10.30 ± 0.07
1151	266.80895	65.54695	22.21 ± 0.07	21.59 ± 0.08	73.8 ± 5.7	0.98 ± 0.24	10.78 ± 0.03
1187	266.77843	65.54844	22.51 ± 0.10	22.12 ± 0.13	31.7 ± 6.4	0.34 ± 0.23	10.69 ± 0.03
1193	266.85794	65.54868	22.54 ± 0.10	21.82 ± 0.10	82.5 ± 7.6	0.85 ± 0.24	10.21 ± 0.06
1247	266.90870	65.55051	22.85 ± 0.13	22.01 ± 0.12	87.3 ± 9.0	0.83 ± 0.26	10.10 ± 0.07
1248	266.81848	65.55068	21.61 ± 0.04	21.19 ± 0.06	49.8 ± 2.6	1.77 ± 0.30	11.28 ± 0.01
1249	266.82366	65.55023	22.43 ± 0.09	21.70 ± 0.09	64.2 ± 4.5	1.43 ± 0.32	10.87 ± 0.03
1259	266.91055	65.55101	21.53 ± 0.04	21.10 ± 0.05	30.2 ± 2.2	1.13 ± 0.28	11.32 ± 0.01
1263	266.63926	65.55091	23.88 ± 0.31	22.32 ± 0.15	309.2 ± 59.5	0.75 ± 0.23	9.93 ± 0.15
1292	266.87637	65.55294	21.52 ± 0.04	21.09 ± 0.05	50.8 ± 1.9	3.26 ± 0.39	11.41 ± 0.01
1304	266.78208	65.55290	22.95 ± 0.14	22.19 ± 0.14	101.7 ± 12.0	0.71 ± 0.24	10.23 ± 0.07
1314	266.78424	65.55358	23.29 ± 0.19	22.55 ± 0.19	170.4 ± 25.7	0.64 ± 0.24	10.07 ± 0.09
1338	266.84831	65.55210	23.23 ± 0.18	22.56 ± 0.19	382.4 ± 53.3	1.31 ± 0.29	9.95 ± 0.10
1339	266.84808	65.55223	23.61 ± 0.25	22.51 ± 0.18	796.6 ± 221.8	1.07 ± 0.25	10.10 ± 0.09
1369	266.81018	65.55505	23.19 ± 0.18	22.55 ± 0.19	73.6 ± 13.8	0.36 ± 0.21	9.93 ± 0.09
1400	266.71106	65.55620	23.07 ± 0.16	22.22 ± 0.14	119.2 ± 13.6	0.77 ± 0.24	10.41 ± 0.06
1412	266.80336	65.55674	22.79 ± 0.12	22.20 ± 0.14	58.2 ± 8.2	0.54 ± 0.25	10.70 ± 0.04
1456	266.72274	65.55935	22.89 ± 0.14	22.09 ± 0.13	98.3 ± 11.0	0.70 ± 0.23	10.43 ± 0.05
1461	266.90942	65.55982	22.52 ± 0.10	21.59 ± 0.08	102.4 ± 5.8	2.00 ± 0.33	10.85 ± 0.03
1502	266.87502	65.56179	22.82 ± 0.13	22.04 ± 0.12	158.6 ± 14.9	1.12 ± 0.26	10.31 ± 0.07
1509	266.73619	65.56193	22.67 ± 0.11	21.55 ± 0.08	124.0 ± 7.9	1.66 ± 0.28	10.46 ± 0.04
1521	266.64455	65.56226	22.25 ± 0.08	21.19 ± 0.06	144.1 ± 6.9	2.00 ± 0.25	10.87 ± 0.02
1554	266.68226	65.56372	22.34 ± 0.08	21.38 ± 0.07	178.8 ± 9.0	2.37 ± 0.28	10.66 ± 0.03
1555	266.68152	65.56408	22.85 ± 0.13	21.77 ± 0.10	165.7 ± 11.3	1.94 ± 0.31	10.87 ± 0.04
1567	266.68369	65.56430	21.97 ± 0.06	21.16 ± 0.06	94.7 ± 4.0	2.41 ± 0.30	11.00 ± 0.02
1576	266.69107	65.56451	22.77 ± 0.12	22.14 ± 0.13	116.1 ± 11.6	0.90 ± 0.25	10.48 ± 0.05
1887	266.76772	65.57359	22.57 ± 0.10	22.06 ± 0.12	56.2 ± 6.2	0.82 ± 0.29	10.38 ± 0.05
2126	266.69413	65.50960	22.81 ± 0.13	21.91 ± 0.11	86.8 ± 7.5	1.11 ± 0.29	10.47 ± 0.04

Notes.
[a] The $M_\star$ uncertainties provided here are based solely on the photometric uncertainties in K_s-band. We note, however, that the uncertainties in $M_\star$ could potentially be dominated by the systematic uncertainties associated with the derivation of $M_\star$ using the one-color method (typically ±0.2 dex; see Koyama et al. 2013b).
[b] The ID 1043 is the radio galaxy 4C 65.22 at $z = 1.52$ (i.e., the primary target of this study).

yielding the expected contamination rate of ∼0.8 arcmin^{-2}. Based on this estimate, we expect ∼0.6 galaxies in the central 250 kpc region. Therefore, the central 250 kpc region of 4C 65.22 field is indeed over-dense by a factor of ∼30 times compared to the control field (see also Section 4). We also expect ∼22 galaxies within $4' \times 7'$ MOIRCS FoV. The number density of the photo-z members in the 4C 65.22 field is still significantly higher than general field (by a factor of ∼3 times), but this analysis suggests that the over-density is diluted when averaged over the FoV.

For SF galaxies, the photometric redshifts may be much less reliable because of their flat featureless broad-band spectral energy distributions (SEDs). We find that only 20 Hα emitters (45%) satisfy the photo-z criteria of $1.3 < z_{\rm phot} < 1.7$ (see the blue-hatched histograms in Figure 3). In particular, we find that the photometric redshift does not work well for Hα emitters with red optical colors, and that the photo-z errors of such red emitters tend to be slightly larger than those of blue emitters. This probably reflects the well-known age/dust degeneracy, making it extremely difficult to construct a complete sample of SF galaxies using a limited set of broadband filters. We remind the reader that this point is an important advantage of the narrow-band survey: it allows us to construct a clean SF galaxy sample within a narrow redshift slice at a

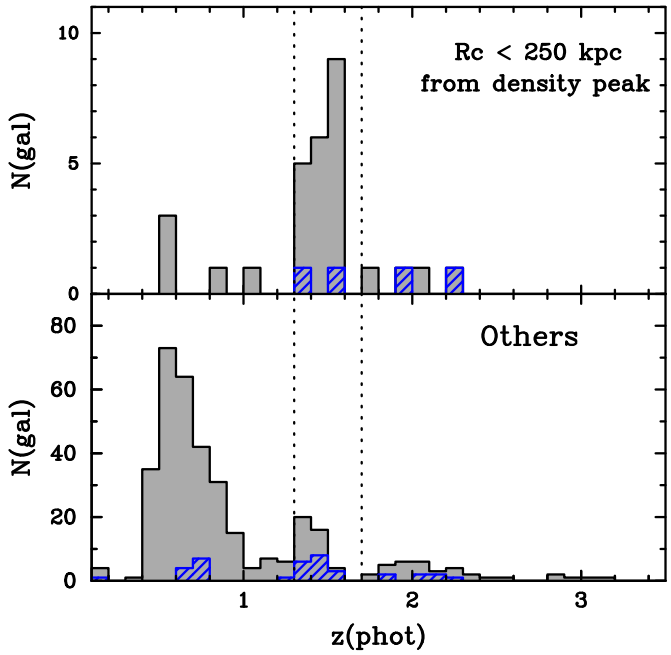

Figure 3. $z_{\rm phot}$ distribution of galaxies for those with $z_{\rm phot} < 3.5$ located within 250 kpc from the density peak (top) and those outside this annulus (bottom), showing a clear redshift spike at $z \sim 1.5$ in the 4C 65.22 field. The dotted lines at $z_{\rm phot} = 1.3$ and 1.7 show the criteria of photo-z member selection applied in this paper. The blue hatched histogram shows the $z_{\rm phot}$ distribution for the Hα emitters selected in Section 3.1. The photo-z accuracy for SF galaxies should be less reliable, but we emphasize that the primary aim of photo-z is to select passive galaxies without Hα emission.

(A color version of this figure is available in the online journal.)

high completeness level (e.g., Kodama et al. 2004; Koyama et al. 2010). In the case of our current data set, ∼55% of SF galaxies might have been missed out with the photo-z selection alone, but those galaxies are now rescued with our NB-based approach.

In summary, we selected the final member galaxies with the following two criteria. First, we select 61 galaxies with $1.3 < z_{\rm phot} < 1.7$. Second, we include all 44 Hα emitters (selected in Section 3.1) regardless of their photometric redshifts. Note that 20 out of the 44 Hα emitters satisfy the above photo-z criteria as well. In these ways, our final member catalog contains a total of 85 galaxies, and this sample will be used in the remainder of this paper. We note that a fraction of the selected Hα emitters might be active galactic nuclei (AGNs). In general, the fraction of AGNs in Hα-selected galaxies at $z \gtrsim 1$ is expected to be ∼10%–15% (Garn et al. 2010; Sobral et al. 2013). However, unfortunately, it is not possible to quantify the AGN contribution in our own sample without multi-wavelength imaging/spectroscopic follow-up observations. In particular, the environmental dependence of the AGN activity in the distant universe is still an open question and is beyond the scope of this paper.

4. DISCOVERY OF A RICH CLUSTER AT $z = 1.52$

4.1. Spatial Distribution of Galaxies Around 4C 65.22

Based on the sample selection described in Section 3, we here report the discovery of a strong over-density of $z \sim 1.5$ galaxies around the radio galaxy 4C 65.22. In Figure 4, we show the spatial distribution of the selected member galaxies. We here plot photo-z-selected galaxies (with $1.3 < z_{\rm phot} < 1.7$; black circles) and the Hα emitters (blue squares). The member galaxies on the red sequence ($z' - J > 1.45$; see Section 4.2) are marked with red symbols. It is evident that there is a clear density peak of $z \sim 1.5$ galaxies near the radio galaxy. The radio galaxy (shown with a yellow star in Figure 4) is located at ≈140 kpc away from the density peak, not in the very center of the core.

We already showed in Figure 3 a clear redshift spike at $z_{\rm phot} \sim 1.5$ within $r_c < 250$ kpc from the density peak. This result does not change even if we consider "all" member galaxies including Hα emitters. The number density of all the member galaxies (i.e., photo-z member and Hα emitters) within the 250 kpc circle is 28.9 arcmin^{-1}, which is a factor of >10 times higher than the average in the outer field (2.3 arcmin^{-2}). We note that a small $z_{\rm phot}$ peak at $z \sim 1.5$ can also be seen in the bottom panel of Figure 3. This probably reflects the presence of large-scale structures extending beyond the 250 kpc circle. Although we need spectroscopic follow-up observation to confirm such relatively poor structures, it is highly possible that some of the small groups as well as the filamentary structures traced by Hα emitters seen in Figure 4 are really associated with the central cluster.

4.2. Red-sequence Galaxies Dominating the Cluster Core and the Deficit of Low-mass Blue Galaxies

Another important result drawn from Figure 4 is that the cluster central region ($r_c \lesssim 250$ kpc) is clearly dominated by red-sequence galaxies without Hα emission (see also Figure 5 for a three-color representation of our rzH images in the central cluster region). Interestingly, this "suppression radius" of ∼200 kpc is consistent with that reported in another X-ray-selected rich cluster at a similar redshift (e.g., Bauer et al. 2011b), suggesting that this newly discovered system is a well-evolved rich galaxy cluster at $z = 1.5$. The presence of a number of Hα emitters (at $1.51 \leqslant z \leqslant 1.54$) surrounding the core further supports our discovery of the rich cluster associated with the radio galaxy. We note that no extended X-ray emission is reported in this field so far; e.g., by the *ROSAT* all-sky cluster survey (Böhringer et al. 2000). This is not surprising given the shallowness of the all-sky survey data. However, it would be highly possible that we can detect an extended X-ray emission associated with this cluster if we can perform a deep X-ray follow-up observation in the future.

In Figure 6, we show color–magnitude diagrams for galaxies located at $r_c < 250$ kpc and those outside this annulus. An interesting feature recognized in this plot is the clear "deficit" of blue galaxies in the central cluster region ($r_c < 250$ kpc), in stark contrast to the outer field. There still exist a few Hα emitters within the $r_c = 250$ kpc circle, but these Hα-emitting galaxies in the cluster core region show redder colors than typical Hα emitters in the field environment. This clear lack of low-mass blue galaxies may represent an accelerated galaxy evolution in high-z cluster environments; it is most likely explained that blue SF galaxies falling into the cluster are quickly transformed into red/massive quiescent population. It is also likely that the quenching process accompanies a quick mass growth via, e.g., mergers or galaxy–galaxy interactions, otherwise we cannot fully explain the deficit of low-mass blue galaxies and the excess of red massive galaxies in the cluster core region at the same time. In Figure 6, the red sequence is only visible in its bright end, consistent with some recent studies of $z \sim 1$ clusters (e.g., Koyama et al. 2007; Stott et al. 2007). The lack of the faint end of the red sequence is unlikely due to the selection effect: we

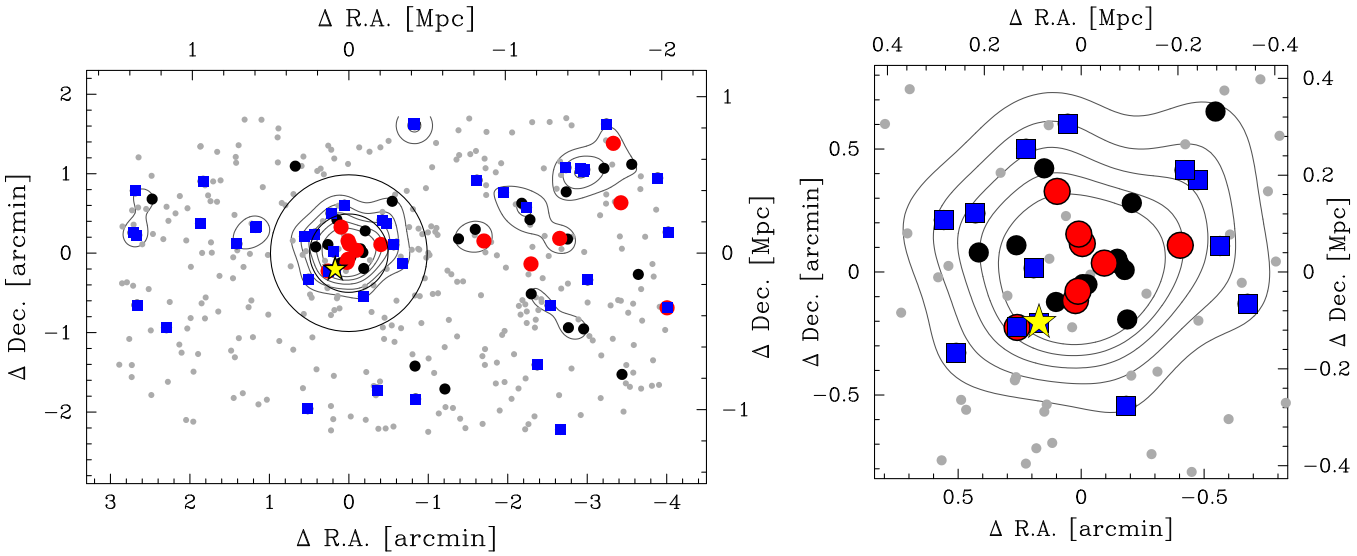

Figure 4. Two-dimensional map of galaxies around 4C 65.22 over the entire MOIRCS FoV ($4'\times7'$; left panel) and the $100''\times100''$ close-up view around the density peak (right panel). The gray dots, black circles, and blue squares show all NB-detected sources, photo-z-selected galaxies with $1.3 \leqslant z_{\rm phot} \leqslant 1.7$, and the H$\alpha$ emitters at $z = 1.5$, respectively. The red symbols show the galaxies on the red sequence. The red-sequence galaxies are strongly clustered near the radio galaxy (yellow star), and Hα emitters tend to be located in the cluster outskirts. The contours show 1, 2, 3, 4, 5σ significance of the over-density calculated with all member galaxies: we applied Gaussian smoothing ($\sigma = 0.1$ Mpc) on each galaxy and combine the tails of Gaussian wings to measure local density at a given point. The (0,0) point of this plot shows the density peak (R.A. = $17^{\rm h}47^{\rm m}12.3^{\rm s}$, decl. = $+65^{\rm d}32^{\rm m}48^{\rm s}$). The solid circles in the left panel show 250 and 500 kpc from the density peak.

(A color version of this figure is available in the online journal.)

Figure 5. False-color image of the 4C 65.22 field created with $r'z'H$-band data. The size of this image is $100''\times100''$, same as the right panel of Figure 4. North is up and east is to the left.

(A color version of this figure is available in the online journal.)

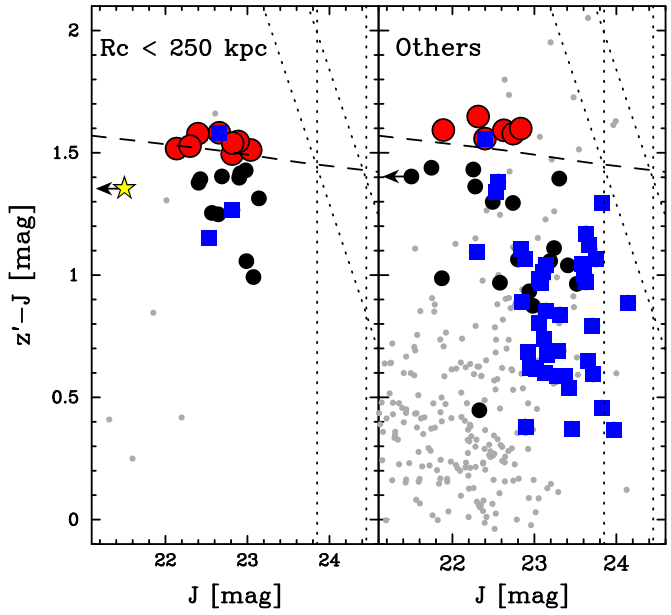

Figure 6. Color–magnitude diagram for all NB-selected sources within 250 kpc from the density peak (left) and outside this radii (right). Black circles show the member galaxies, while blue squares show Hα emitters. The red circles are member galaxies with $z' - J > 1.45$ (identical to the red symbols in Figure 4). The vertical and slanted dotted lines show 3 and 5σ limiting magnitudes in z' and J, respectively. The dashed line shows the location of the red sequence (assuming $z_f = 5$) modeled by Kodama et al. (1998). Interestingly, low-mass blue galaxies are clearly deficient in the cluster core region.

(A color version of this figure is available in the online journal.)

verified that the number of faint red galaxies does not increase even if we use J-band detected catalog instead of NB-selected catalog.

We also show in Figure 7 the cumulative (and differential) fraction of each population in our total sample as a function of the distance from the density peak out to $r_c = 1$ Mpc. This plot further supports our claim that red galaxies are strongly clustered within $r_c \sim 250$ kpc. It is evident that the fraction of red galaxies sharply drops at $r_c \sim 200$–300 kpc, which coincides with where we see the dramatic increase in Hα emitters and blue galaxies. The Kolmogorov–Smirnov test (KS test) suggests with a >99.9% confidence level that the distributions of red galaxies and Hα emitters (or blue galaxies) are drawn from a different parent population. We therefore conclude that most blue SF galaxies falling into the highest-density cluster core are forced

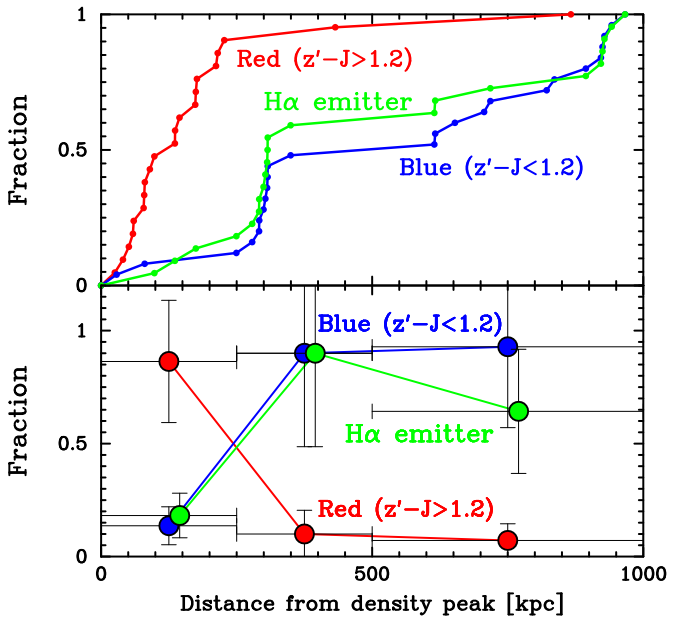

Figure 7. Cumulative (top) and differential (bottom) plot of the fraction of each population to the total galaxy sample studied here as a function of the distance from the density peak. This plot clearly demonstrates that the dominant galaxy population sharply changes at around $r_c \sim 200$–300 kpc. In the bottom panel, the vertical error bars represent 1σ uncertainty from Poisson statistics, while the horizontal error bars show the bin size used for calculation. We applied a small shift for the symbols for clarity. Most blue galaxies and Hα emitters are overlapped with each other, but they are not completely overlapped: i.e., there are some red Hα emitters as well as blue galaxies without Hα emission.

(A color version of this figure is available in the online journal.)

to migrate toward the red sequence, resulting in a clear deficit of low-mass blue galaxies in the central part of this cluster.

5. GALAXY PROPERTIES VERSUS ENVIRONMENT

5.1. Color–Density and M_*–Density Relation

Using the newly discovered cluster field as a laboratory, we here take a more detailed look at the environmental dependence of galaxy properties at $z \sim 1.5$. For each member galaxy, we calculate the local surface number density ($\Sigma_{5\mathrm{th}} = 5/\pi r_{5\mathrm{th}}^2$), where $r_{5\mathrm{th}}$ denotes the distance to the fifth-nearest neighbor of each member galaxy. In the following analysis of this paper, we use this local density $\Sigma_{5\mathrm{th}}$ as an environmental index, but our results do not change even if we use $\Sigma_{3\mathrm{rd}}$ or $\Sigma_{10\mathrm{th}}$.

We first focus on galaxy colors. In Figure 8 (left), we show $z'-J$ (rest-frame $U-V$) colors of member galaxies as a function of $\Sigma_{5\mathrm{th}}$. This plot clearly demonstrates that the color–density relation is already in place at $z \sim 1.5$, consistent with the visual impression from Figure 4. We here compute the Spearman's rank correlation coefficient ($\rho = 0.40$). With a sample size of $N_{\mathrm{all}} = 84$, we can conclude that there is a significant correlation between the two variables[9]: a null hypothesis that there is no correlation between $z' - J$ and $\Sigma_{5\mathrm{th}}$ is ruled out at >99% confidence level.

The correlation becomes much less significant when we consider only Hα emitters. In this case, the Spearman's rank correlation coefficient is $\rho = 0.11$. With a sample size of $N_{\mathrm{HAE}} = 43$, we cannot rule out a null hypothesis that there is no significant correlation between $z' - J$ and $\Sigma_{5\mathrm{th}}$ for Hα emitters. Therefore, we suggest that the color–density relation is primarily driven by passive red galaxies in the highest-density cluster core, equivalently by the lack of blue galaxies in the highest-density region. We note, however, that there is a weak correlation between the EW(Hα+[N II]) and galaxy colors in the sense that redder Hα emitters tend to have lower EW (see the blue squares in Figure 8, where we use different symbol size for high-EW/low-EW emitters). In other words, our definition of the Hα emitters ($H-\mathrm{NB1657} > 0.2$) may potentially fail to select low-EW (red) Hα emitters. Therefore, we need to keep in mind that the results on the color–density relation amongst Hα emitters could be highly sensitive to the EW cut used for the sample selection.

It is possible that the color–density relation is partly produced by the correlation between galaxy stellar mass and environment. We here investigate the environmental dependence of stellar masses ($M_\star$) of the member galaxies. The $M_\star$ of galaxies are derived using K_s-band photometry with $M_\star/L_{\mathrm{K_s,obs}}$ correction based on the $z' - K_s$ color as the following.

$$\log(M_\star/10^{11} M_\odot)_{z=1.5} = -0.4(K_s - 21.53) + \Delta M_\star, \quad (1)$$

where $\Delta M_\star = 0.095$–$1.003 \times \exp(-0.807 \times (z' - K_s))$ indicates the M/L correction value. These conversion equations are derived using the model galaxies developed by Kodama et al. (1998) assuming Salpeter (1955) initial mass function (IMF). It is demonstrated that this "one-color method" can provide reasonable $M_\star$ values out to $z \sim 2$ (see Koyama et al. 2013b).

In Figure 8 (right), we plot the derived $M_\star$ as a function of $\Sigma_{5\mathrm{th}}$. Our data suggest that there exists a weak $M_\star$–density relation in the observed field, again driven by the massive galaxies in the highest-density cluster core. By computing the Spearman's rank correlation coefficient ($\rho = 0.23$), and with a sample size of $N_{\mathrm{all}} = 84$, we can rule out the null hypothesis that there is no $M_\star$–$\Sigma_{5\mathrm{th}}$ relationship with ≈97% confidence level. However, if we focus only on the Hα emitters, the Spearman's rank correlation coefficient is $\rho = 0.11$, suggesting no significant correlation between the two variables with the sample size of $N_{\mathrm{HAE}} = 43$. Our data thus suggest that the color–density and $M_\star$–density relation are already in place at $z \sim 1.5$, mostly driven by passive red/massive galaxies in the highest-density region. However, the correlations almost disappear when we consider only SF galaxies.

5.2. SFR–Density and SSFR–Density Relation

An important advantage of the NB Hα survey is that we can measure Hα flux of all emitters within the observed FoV. We here describe how we derive the Hα-based SFRs of Hα emitters, and then describe how the derived SFRs depend on environment. First of all, we calculate the Hα+[N II] line flux ($F_{\mathrm{H\alpha+[N\,II]}}$), continuum flux density (f_c) and rest-frame EW ($\mathrm{EW_{rest}}$) of each Hα emitter based on its broad-band and narrow-band photometry with the following equations:

$$F_{\mathrm{H\alpha+[N\,II]}} = \Delta_{\mathrm{NB}} \frac{f_{\mathrm{NB}} - f_H}{1 - \Delta_{\mathrm{NB}}/\Delta_H} \quad (2)$$

$$f_c = \frac{f_H - f_{\mathrm{NB}}(\Delta_{\mathrm{NB}}/\Delta_H)}{1 - \Delta_{\mathrm{NB}}/\Delta_H} \quad (3)$$

$$\mathrm{EW_{rest}}(\mathrm{H\alpha + [N\,II]}) = (1+z)^{-1} \frac{F_{\mathrm{H\alpha+[N\,II]}}}{f_c}. \quad (4)$$

[9] In the following statistical tests, we do not use the radio galaxy itself because its physical quantities such as color, mass, and SFR are contaminated by unpredictable central AGN activity. However, our results do not change even if we include it in the analyses.

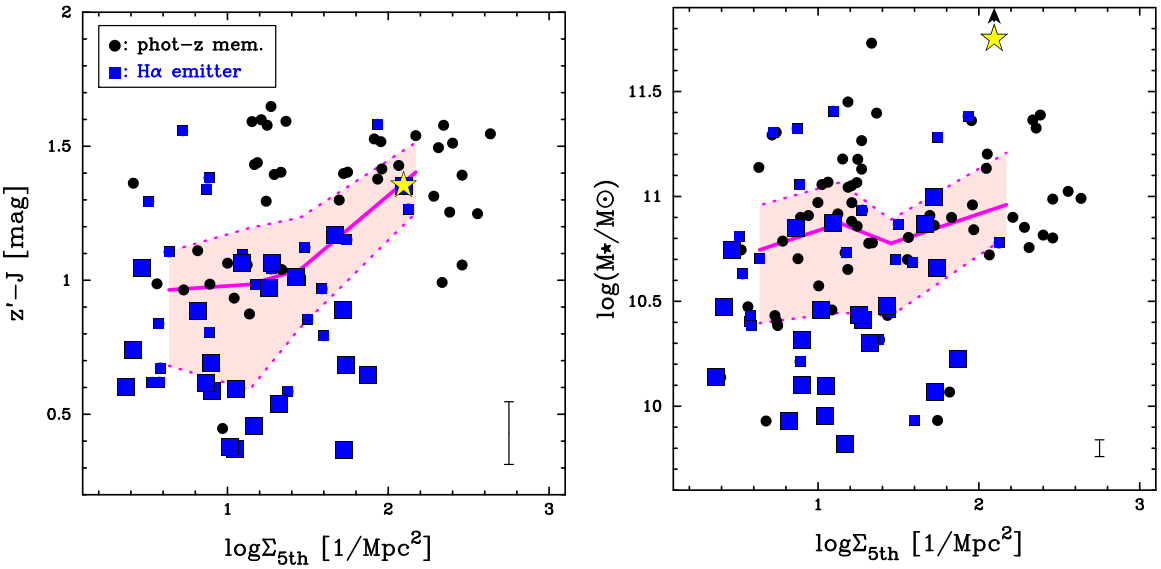

Figure 8. Color–density and $M_\star$–density relation for $z \sim 1.5$ galaxies around the radio galaxy 4C 65.22. The blue squares and black circles show the selected member galaxies with and without Hα emission, respectively. We split the Hα emitter sample into two equal-sized bins based on EW_{rest}(Hα+[N II]), and use large and small squares for high-EW and low-EW emitters, respectively. We also show the running median in each plot calculated by splitting the sample into four equal-sized bins (magenta solid line), as well as the 25% and 75% distribution by the pink shaded region. These plots show that the color and $M_\star$ are both correlated with the local galaxy density, but we note that the environmental trends become less prominent when we consider only Hα emitting galaxies. Typical uncertainties are indicated at the bottom right corner of each panel. The uncertainty in $M_\star$ shown here simply reflects the K_s-band photometric errors (hence lower limits), but we note that the systematic uncertainties accompanied by the derivation of $M_\star$ with the one-color method (i.e., Equation (1)) may potentially dominate the $M_\star$ uncertainty (typically $\pm$0.2 dex as discussed by Koyama et al. 2013b).

(A color version of this figure is available in the online journal.)

The Δ_H (=0.28 μm) and Δ_{NB} (=0.0195 μm) are the FWHMs of the broad-band (H) and NB1657 filters, f_H and f_{NB} are the flux densities at H-band and at NB1657, respectively. We then multiply $4\pi\, d_L^2$ by $F_{H\alpha+[N\,II]}$ to derive the luminosity $L_{H\alpha+[N\,II]}$, where d_L is the luminosity distance of 1.109×10^3 Mpc at $z = 1.5$.

We correct for the [N II] line contribution into the total NB fluxes, using the empirical calibration between [N II]/(Hα+[N II]) flux ratio and EW_{rest}(Hα+[N II]) for local SDSS galaxies presented by Sobral et al. (2012). The median of the derived [N II]/(Hα+[N II]) ratio for our Hα emitter sample is 0.19, consistent with the Hα emitter sample at $z = 1.46$ ([N II]/(Hα+[N II])= 0.22) shown by Sobral et al. (2012). Although there remains a large scatter around this relation ($\sim$0.4 dex; e.g., Villar et al. 2008), it is impossible to measure [N II] line flux for all galaxies because it requires deep spectroscopic observation for all of them. Therefore, our procedure is the best effort at this moment, and at least it would be more realistic than the conventional constant (e.g., 30%) correction. We then compute the dust-free Hα-based SFR, $SFR_{H\alpha}$, using the Kennicutt (1998) relation for Salpeter (1955) IMF; $SFR_{H\alpha}(M_\odot\ yr^{-1}) = 7.9 \times 10^{-42}\, L_{H\alpha}(erg\ s^{-1})$. We note that our H$\alpha$ emitter selection criteria shown in Section 3.1 approximately correspond to EW_{rest}(Hα+[N II]) $\gtrsim$ 20 Å and $SFR_{H\alpha} \gtrsim 3\ M_\odot\ yr^{-1}$.

Finally, we correct for the dust extinction effect. We here consider two independent methods to estimate dust extinction at Hα ($A_{H\alpha}$). The first method is to use $A_{H\alpha}$–$M_\star$ relation established for local galaxies by Garn & Best (2010). The $A_{H\alpha}$–$M_\star$ correlation is likely to be unchanged up to $z \sim 1.5$ (Sobral et al. 2012; Ibar et al. 2013), and this method is often used in studies of distant galaxies as a convenient method to predict dust extinction effect for individual galaxies.

The second approach is to use $SFR_{H\alpha}/SFR_{UV}$ ratio for predicting $A_{H\alpha}$. Because Hα is less sensitive to the dust extinction effect than rest-frame UV light, the $SFR_{H\alpha}/SFR_{UV}$ ratio can be used as an indicator of dust attenuation (Buat et al. 2002; Tadaki et al. 2013). In our case, the B-band flux density ($\lambda_{rest} \approx 1800$ Å) can be converted to the rest-frame UV luminosity density, and then we derive SFR_{UV} using Kennicutt (1998) calibration; $SFR_{UV} = 1.4 \times 10^{-28} L_\nu(erg\ s^{-1}\ Hz^{-1})$. The observed $SFR_{H\alpha}/SFR_{UV}$ ratio is translated to the dust extinction value using the following equation:

$$E_{star}(B-V) = \frac{2.5 \times \log(SFR_{H\alpha}/SFR_{UV})}{k_{UV} - k_{H\alpha}/f}, \quad (5)$$

$$A_{H\alpha} = k_{H\alpha} \times E_{star}(B-V)/f. \quad (6)$$

We here adopt $k_{H\alpha} = 3.33$ and $k_{UV} = 9.37$ from Calzetti et al. (2000) law with $R_V = 4.05$. We must treat the extra extinction toward the nebular regions (f value in the above equations) carefully. In the Calzetti et al. (2000) prescription, the f value was shown to be 0.44 (i.e., $A_{H\alpha} = A_{cont}/0.44$). However, recent studies claim that this f value is likely to be different for high-z SF galaxies (e.g., Price et al. 2013). Kashino et al. (2013) empirically linked the $SFR_{H\alpha}/SFR_{UV}$ ratio to $E(B-V)$ for $z \sim 1.3$ SF galaxies. They derived the best-fitted value of $f = 0.69$, and we adopt this value to our analysis. We note that the method may not be perfect enough (e.g., $SFR_{H\alpha}/SFR_{UV}$ flux ratio could depend on galactic age; see Wuyts et al. 2013 for a detailed discussion), but we expect this method is more realistic than the simple $M_\star$-dependent correction shown above.

In Figure 9 (left), we plot the derived $A_{H\alpha}$ values against their stellar mass for all Hα emitters. The extinction effect (derived by the $SFR_{H\alpha}/SFR_{UV}$ ratio) increases with stellar mass, showing a reasonable agreement with the local $A_{H\alpha}$–$M_\star$ relation. Also, the derived $A_{H\alpha}$ values are higher for red Hα emitters (see the middle panel of Figure 9), suggesting the redder Hα emitters tend to be dustier. It may be interesting to note that there is a large scatter around the $A_{H\alpha}$–$M_\star$ relation, and that there exist some exceptionally dusty galaxies

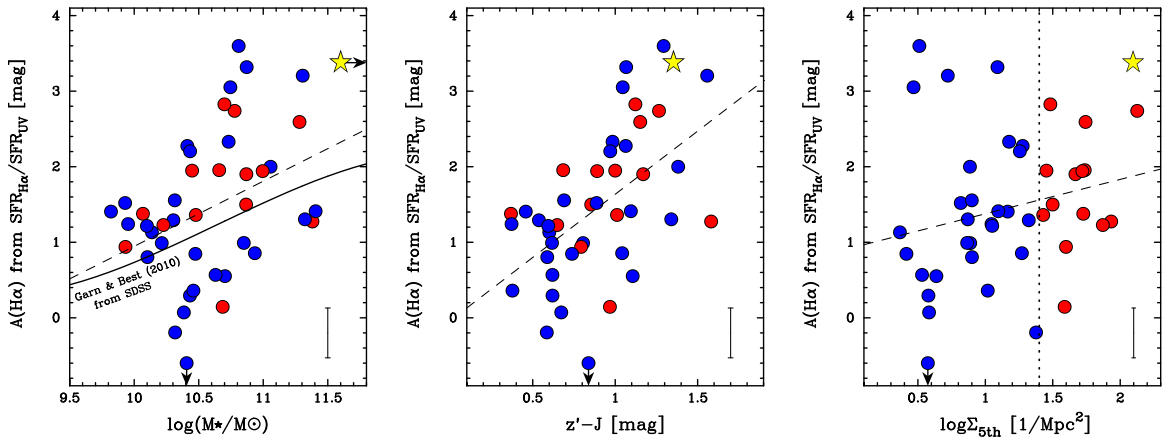

Figure 9. $A_{\rm H\alpha}$ values derived from SFR(Hα)/SFR(UV) ratio against their stellar mass (left), $z'-J$ colors (middle), and environment (right). The red and blue symbols show the Hα emitters in the high-density ($\log\Sigma_{\rm 5th} \geqslant 1.4$; top $\sim$1/3) and in low-density ($\log\Sigma_{\rm 5th} < 1.4$) environment. The yellow star indicates the radio galaxy. In the left panel, we also show the empirical $A_{\rm H\alpha}$–$M_\star$ relation for local star-forming galaxies from Garn & Best (2010), accounted for IMF difference. Our Hα emitter sample at $z = 1.52$ also shows that the $A_{\rm H\alpha}$ value increases with $M_\star$, but there seems to be a large scatter around the $A_{\rm H\alpha}$–$M_\star$ relation. In each plot, the dashed line shows the simple best-fitted relation, and the typical error bar size is shown in the bottom right part of each plot. Interestingly, there is a weak positive correlation between $A_{\rm H\alpha}$ and $\Sigma_{\rm 5th}$ (although only with $\sim 1\sigma$ significance), suggesting star-forming galaxies in high-density environment may be more highly obscured by dust.

(A color version of this figure is available in the online journal.)

with $A_{\rm H\alpha} \gtrsim 3$ mag, which cannot be identified with the simple $M_\star$-dependent correction.[10] Also, there may be a weak correlation between $A_{\rm H\alpha}$ and environment for the same Hα emitters sample (see Figure 9, right). Although the statistical significance is low (only $\sim 1\sigma$ level) and there is a large uncertainty in deriving $A_{\rm H\alpha}$ of individual galaxies, this result may suggest that SF galaxies in high-density environments tend to be more highly obscured by dust (by $\sim$0.5 mag level) than field counterparts. This is qualitatively consistent with our recent study (Koyama et al. 2013b), where we showed a higher dust extinction of cluster galaxies with a 24 μm stacking analysis for $z = 0.4$ galaxies.

Finally, we show in Figure 10 the SFRs and specific SFRs (SSFR = SFR/$M_\star$) of all Hα emitters as a function of local galaxy density ($\log\Sigma_{\rm 5th}$ measured with all member galaxies). The left and right panels show the results based on the two independent dust extinction correction described above. We do not find any significant SFR–density or SSFR–density correlation in any of the four panels in Figure 10, suggesting that SF activity of SF galaxies does not significantly change with environment. By computing the Spearman's rank correlation coefficients with a sample size of $N_{\rm HAE} = 43$, we cannot reject a null hypothesis that there is no significant relationship between the two variables in any of these four panels. We caution that our results are based on the purely Hα-selected galaxies (i.e., for SF galaxy population). The clear excess of non-Hα-emitting red-sequence galaxies in the very high-density region (as shown in Figures 4–6) implies an anti-correlation between (S)SFR and environment, although we cannot measure SFRs of galaxies without Hα emission.

5.3. Star Formation Main Sequence

The important goal of this study is to test the environmental dependence of the SF main sequence at $z \sim 1.5$ using the Hα-selected galaxies in the newly discovered cluster field. In Figure 11, we show the SFR–$M_\star$ diagrams for Hα emitters in the 4C 65.22 field. The left and right panels show the result from different dust extinction correction: derived from $M_\star$ (left panel) and from $\rm SFR_{H\alpha}/SFR_{UV}$ ratio (right panel). In this plot, the Hα emitters in high-density environment ($\log\Sigma_{\rm 5th} > 1.4$; top $\sim$1/3) are shown with the red circles, while the other Hα emitters are shown with blue circles. Regardless of the dust extinction correction procedure, we find that the location of the SF main sequence is independent of environment at $z \sim 1.5$.

In the bottom panels of Figure 11, we also show the distribution of SFR offsets from the main sequence ($\Delta\rm MS_{offset}$) for galaxies in high-density (red filled histogram) and low-density environment (blue hatched histogram). Again, we do not see any strong difference between the two environment samples: the KS test suggests that it is likely that the two distributions are drawn from the same parent population in either case of the dust extinction procedure, further supporting our conclusion that the location of the SF main sequence does not significantly change with environment. One potentially interesting finding from Figure 11 is that the Hα emitters in the higher-density region (red symbols) tend to populate the higher envelope of the SF main sequence in the massive end (with $\log(M_\star/M_\odot) > 10.5$). We attempt to quantify this trend by calculating the fraction of galaxies with $\log(\Delta\rm MS_{offset}) > 0.3$ (i.e., galaxies with boosted activity). The fraction turns out to be 56% $\pm$ 31% and 33% $\pm$ 19% for high- and low-density sample, respectively. The error bars are clearly large due to the limited sample size, preventing us from drawing any firm conclusion. However, at least to say, those massive galaxies with boosted activity in high-z cluster environments should be an interesting population under the influence of environmental effects.

Finally, we investigate the origin of the scatter of the $\Delta\rm MS_{offset}$ value within our observed field. In the top panel of Figure 12, we plot the spatial distribution of the Hα emitters by dividing the sample into three categories based on the $\Delta\rm MS_{offset}$ value: "bursty" galaxies ($\log\Delta\rm MS_{offset} > 0.3$), "normal" galaxies ($-0.3 < \log\Delta\rm MS_{offset} < 0.3$), and "semi-passive" galaxies ($\log\Delta\rm MS_{offset} < 0.3$). The sample is of course small, but it may be interesting to note that the northwest group located $\sim$1 Mpc away from the main body of the cluster tends to have a large number of "bursty" galaxies, implying that star-burst activities

[10] We note that there are two Hα emitters showing $A_{\rm H\alpha} < 0$ (i.e., $\rm SFR_{H\alpha}/SFR_{UV} < 1$). One of these sources (ID 930) is consistent with $A_{\rm H\alpha} = 0$ within its error bar (probably a dust-free galaxy), whilst the other source (ID 13) shows an unrealistic negative $A_{\rm H\alpha}$ value. This is because the B-band flux of ID 13 is contaminated by its close companion galaxy (due to the poorer PSF size of our B-band data). Although we do not remove this source from our analyses, it does not affect our conclusion at all.

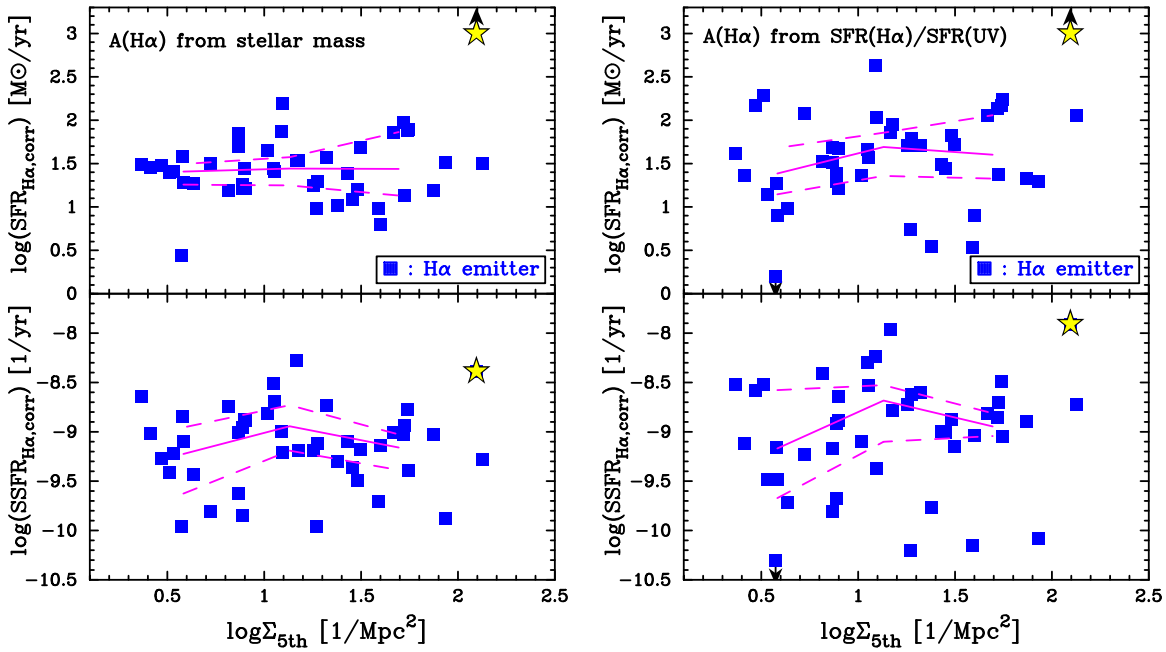

Figure 10. SFR–density (top) and SSFR–density (bottom) relation for Hα emitters at $z = 1.5$. The left and right panels show the result based on the different dust extinction procedure. Only Hα emitters are plotted on these diagrams because it is impossible to measure SFRs of non-Hα emitters. The yellow star indicates the radio galaxy, which will be excluded from the statistical test performed in this paper. Regardless of the dust extinction correction procedure, there is no clear environmental dependence of SFR or SSFR when we consider only star-forming galaxies. The running median (as well as the 25% and 75% distribution) are shown in each plot.

(A color version of this figure is available in the online journal.)

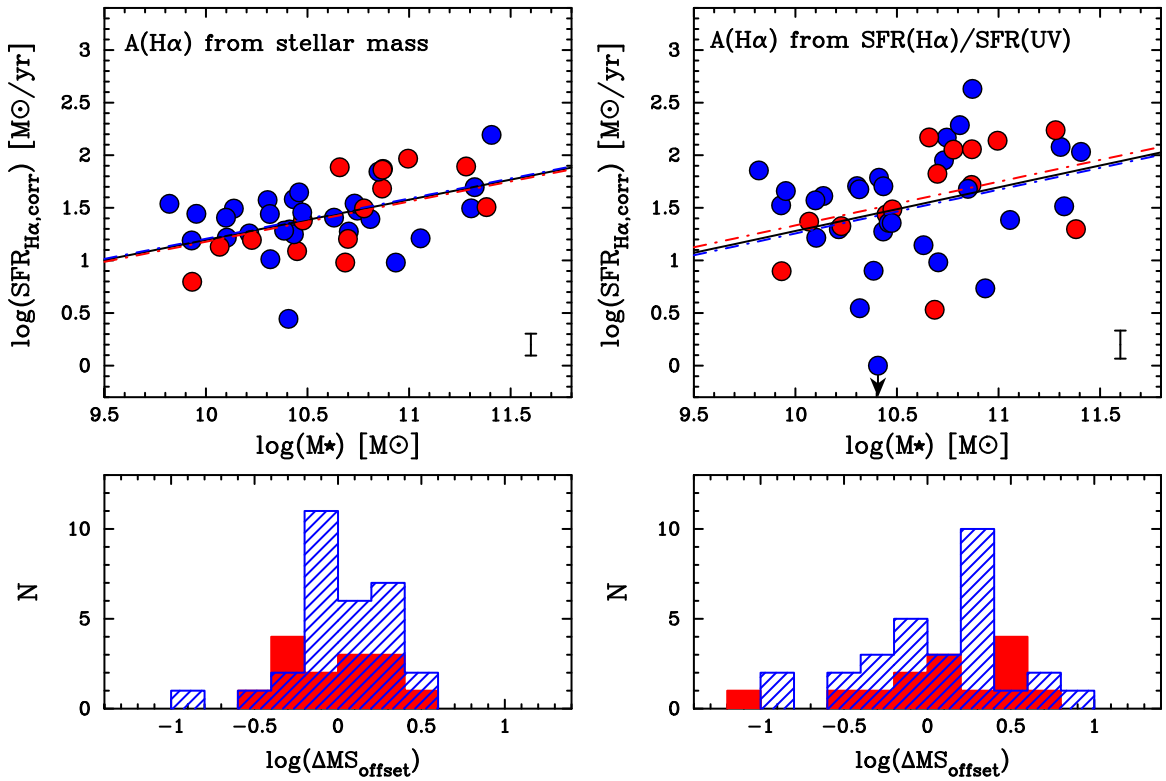

Figure 11. SFR–$M_\star$ diagram for Hα emitters at $z \sim 1.5$ in the field of 4C 65.22. The left panel shows the result with the $M_\star$-dependent extinction correction shown by Garn & Best (2010), while the right panel shows the result with extinction correction from SFR(Hα)/SFR(UV) ratio. The radio galaxy is not plotted on this diagram given the large uncertainty for deriving both $M_\star$ and SFR. For each plot, we show the best-fitted SFR–$M_\star$ relation for all emitters (black solid line), for those in high-density environment ($\log \Sigma_{5th} \geqslant 1.4$; red dot–dashed line) and low-density environment ($\log \Sigma_{5th} < 1.4$; blue dot–dashed line). In the bottom, we show the histograms of the SFR offset from the black line in the top panels (ΔMS_{offset}) for each environmental bin; red filled histogram for high-density and blue shaded histogram for low-density environment.

(A color version of this figure is available in the online journal.)

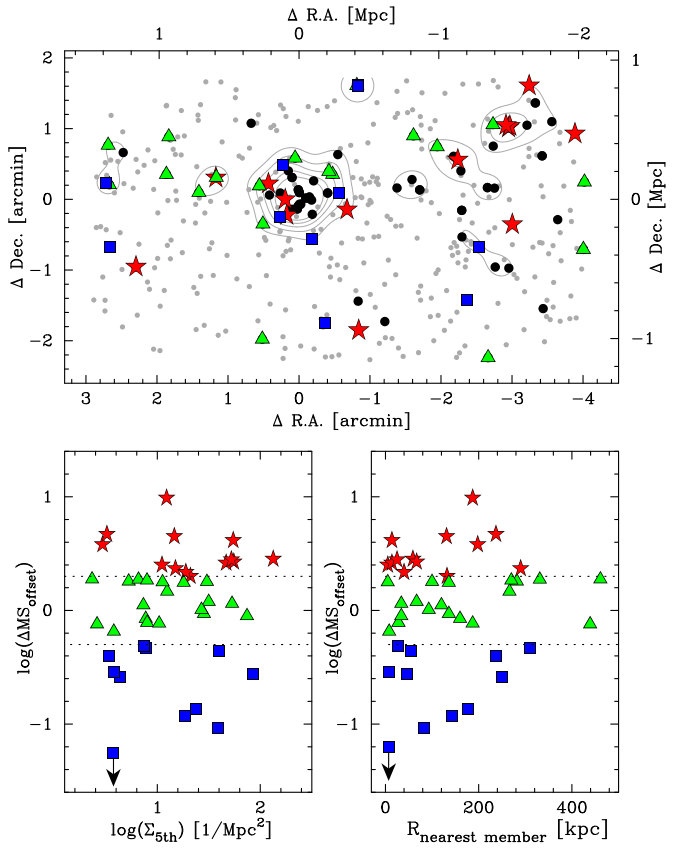

Figure 12. Top: same plot as Figure 4, but the Hα emitters are divided into three categories based on the offset from the main sequence (ΔMS). The red stars, green triangles, and blue squares show Hα emitters with $\log(\Delta\mathrm{MS}) > 0.3$, with $-0.3 < \log(\Delta\mathrm{MS}) < 0.3$, and with $\log(\Delta\mathrm{MS}) < -0.3$, respectively. The black circles show the other member galaxies without Hα emission. Bottom: the $\log(\Delta\mathrm{MS})$ values of Hα emitters as a function of $\log \Sigma_{5\mathrm{th}}$ (left) and the distance to the nearest neighbor (R_{nearest}; right). Note that the ΔMS values shown in this plot are calculated with the dust extinction correction derived from $\mathrm{SFR_{H\alpha}/SFR_{UV}}$, and the $\Sigma_{5\mathrm{th}}$ and R_{nearest} are computed with all member galaxies (including non-Hα emitters).

(A color version of this figure is available in the online journal.)

are most frequently triggered in poor group environments. In contrast, we can see a mix of bursty/normal/semi-passive population in the periphery of the cluster core. The local density ($\Sigma_{5\mathrm{th}}$) of galaxies in the cluster periphery is similar to those in the north-west group, making it hard to identify the site of starburst activity with the local density approach alone (see the bottom left panel of Figure 12).

To further investigate the environmental origin of the scatter of the SF main sequence, we show in the bottom right panel of Figure 12 the ΔMS values as a function of the distance to the nearest neighboring member galaxy (R_{nearest}). In this plot, we find a tentative hint that galaxies having a close companion (with $\lesssim$200 kpc) tend to show a larger scatter around the main sequence, whilst isolated galaxies tend to be located on the main sequence. The sample is small, but this plot may suggest a potential link between the galaxy–galaxy encounter and the deviation around the SF main sequence—i.e., a galaxy tends to show a boosted/truncated SF activity once they become a satellite of another galaxy (cf. Park & Hwang 2009; Hwang et al. 2011). However, because of the mixture of bursty/normal/passive population, we cannot detect an environmental variation in the location (or zero point) of the SF main sequence.

6. DISCUSSION

6.1. Galaxy Population in $z \gtrsim 1.5$ Clusters

It has long been an observational challenge to find a galaxy cluster at $z \gtrsim 1.5$ until recently. However, an increasing number of studies have identified clusters at such frontier redshifts with various techniques (e.g., Kurk et al. 2009; Santos et al. 2011; Nastasi et al. 2011; Stanford et al. 2012; Muzzin et al. 2013), and the nature of such high-z clusters and their member galaxies are now being investigated. Some studies point out that SF activity in high-z cluster cores are comparable to (or even higher than) general field galaxies (e.g., Hayashi et al. 2010; Hilton et al. 2010; Tran et al. 2010; Tadaki et al. 2012); hence, galaxy clusters at these redshifts are interpreted as being in the "transitional phase" or final quenching period (Hayashi et al. 2011; Brodwin et al. 2013; Smail et al. 2014; Alberts et al. 2014).

Interestingly, our newly discovered cluster reported in this paper more closely resembles $z \lesssim 1$ clusters, characterized by a strong concentration of passive red galaxies in the cluster center and SF population surrounding the core (e.g., Koyama et al. 2010, 2011). Our finding of the suppressed SF activity in the cluster core is also similar to the situation in the well-studied rich cluster XMMU J2235.3−2557 at $z = 1.39$ (Lidman et al. 2008; Bauer et al. 2011b; Grützbauch et al. 2012; Santos et al. 2013). Recently, Tanaka et al. (2013) studied an X-ray-detected $z = 1.6$ group in Chandra Deep Field South. Based on the SED and morphological analyses using the CANDELS data, these authors suggest that most galaxies in this $z \sim 1.6$ group are quiescent early-type systems (with a few of them spectroscopically confirmed). The size of the spatial extension of quiescent galaxies in the system reported by Tanaka et al. (2013) is also qualitatively consistent with that of our newly discovered system at $z = 1.5$ (∼200–300 kpc scale).

In our current work, by utilizing the narrow-band Hα imaging technique, we find a clear "deficit" of blue galaxies in the central cluster region ($r_c < 250$ kpc). We do find a few Hα emitters within the $r_c = 250$ kpc circle, but those Hα emitting galaxies in the cluster core show redder colors than typical blue Hα emitters seen in general field environment (Section 4.2). We anticipate that the clear lack of low-mass blue galaxies in the cluster central region is due to the rapid SF quenching and rapid mass growth triggered by environmental effects. If a low-mass blue galaxy enters a rich cluster environment, its SF activity will soon be quenched. This quenching mechanism should accompany an intense short-lived starburst or merging event, because the red-sequence galaxies dominating the cluster core tend to be much more massive than typical blue SF galaxies in the surrounding field.

6.2. Color–Density, SFR–Density Relation at $z > 1$

The color–density relation has been investigated out to $z \sim 1$ or even beyond (e.g., Kodama et al. 2001; Cucciati et al. 2006; Cooper et al. 2010; Chuter et al. 2011; Quadri et al. 2012). Our data suggest that the color–density relation is already in place around the radio galaxy at $z \sim 1.5$. However, the correlation becomes much weaker once we remove non-Hα-emitting galaxies, suggesting that the color–density relation is a product of passive red-sequence galaxies dominating the highest-density cluster core. A similar result was drawn from morphological analysis of cluster/field galaxies at $z \sim 1.6$ by Bassett et al. (2013). These authors showed that the morphologies of SF galaxies in

cluster and field environments at $z \sim 1.6$ show no significant difference. We note, however, that our data covers only a limited FoV (2.0×3.6 Mpc^2), and it is possible that we do not sample galaxies in very low-density environments. We also note that the definition of the Hα emitters in this study is EW$_{\rm rest}$(Hα+[N II]) $\gtrsim 20$ Å, which might be too large if we consider local SF galaxies (e.g., Kennicutt & Kent 1983). At $z \sim 1.5$, however, it is expected that the EW$_{\rm rest}$(Hα+[N II]) $\gtrsim 20$ Å criterion allows us to select a fairly complete sample of normal main sequence galaxies. Therefore, we do not expect that the EW cut does not make any strong impacts on our results, but we need to keep in mind that our survey can potentially miss low-EW (but still SF) galaxies. This is an inevitable problem associated with any NB-based study, and we need future deep imaging/spectroscopic observations to construct a more complete sample of galaxies down to such less active population.

It is worth mentioning that recent studies on $z > 2$ proto-clusters suggest that SF galaxies in higher-density environments tend to have redder colors, implying a color–density correlation amongst SF galaxies (see Koyama et al. 2013a; Hayashi et al. 2012). Koyama et al. (2013a) showed that most of Hα emitters with red $J - K$ colors in the core of the PKS1138–262 proto-cluster at $z = 2.2$ are very massive system (with $\log M_\star \gtrsim 10^{11} M_\odot$). Such an accelerated galaxy stellar mass growth is also suggested by some recent studies on $z \gtrsim 2$ proto-clusters (Steidel et al. 2005; Hatch et al. 2011; Matsuda et al. 2011; Cooke et al. 2014). In our current analysis, we find a number of red massive galaxies without star formation in the core of the $z \sim 1.5$ cluster. The stellar masses of these passive population are comparable to those of massive SF galaxies in the $z > 2$ proto-cluster environments. If we assume that those massive SF galaxies reported in $z > 2$ proto-cluster environments are the direct progenitors of passive red galaxies seen in the $z \sim 1.5$ cluster core, they are expected to have stopped their SF activity within a relatively short time interval between $z \sim 2$ and $z \sim 1.5$.

There have been a lot of debates on the "reversal" of the SFR–density relation in the distant universe. Elbaz et al. (2007) first noted this possibility with the multi-wavelength data set in the GOODS fields (see also Cooper et al. 2008; Ideue et al. 2009). This reversal of the SF–density relation is still under debate, and it is likely that the results could be uncertain depending on the sample definitions and/or the definitions of environment (Sobral et al. 2011; Patel et al. 2011; Scoville et al. 2013; Ziparo et al. 2013). At least for SF galaxies, recent studies have obtained a similar conclusion that there is no significant SFR–density or SSFR–density correlation amongst SF galaxies (McGee et al. 2011; Peng et al. 2010, 2012; Tadaki et al. 2012; Muzzin et al. 2012). The results drawn from our current work is consistent with those recent studies. We caution that the "flat" SFR–density relation may not hold at $z \gtrsim 2$. As we demonstrated in Koyama et al. (2013a), SF galaxies in proto-cluster environments tend to be more massive than those in under-dense regions. Although most of the Hα emitters in proto-cluster environments tend to be located on the SF main sequence, they are skewed to the massive end of the main sequence; hence their SFRs tend to be higher (on average) than those in general field environments.

6.3. Environmental Impacts on the SF Main Sequence

A vital approach to understanding the environmental effects on SF galaxies is to examine the environmental impacts on the SF main sequence. Recent studies have investigated the SF main sequence mainly for distant field galaxies. Those studies have confirmed the existence of the SF main sequence out to $z \sim 2.5$ or above, but the environmental dependence of SF main sequence is much poorly understood due to the lack of well-defined SF galaxy samples in clusters/groups in the distant universe.

In Koyama et al. (2013b), we studied the environmental dependence of the SF main sequence using our purely Hα-selected galaxy samples at $z = 0.4, 0.8, 2.2$ in distant cluster environments and general field environments. We found that there is no significant environmental variation in the SF main sequence out to $z \sim 2$ (with a difference of $\sim$0.2 dex at maximum). In that work, we used $M_\star$-dependent extinction correction for all Hα emitters, which is reported to be unchanged (at least on average) throughout the cosmic time (Sobral et al. 2012). However, we need to test the validity of this procedure by comparing the results derived with different methods of dust extinction correction. In our current analysis, we test this concern by estimating the Hα dust extinction in a more realistic way using the SFR$_{\rm H\alpha}$/SFR$_{\rm UV}$ ratio. However, we again find that the location of the SF main sequence does not change with environment (with a difference of $\lesssim$0.1 dex level), confirming the conclusion drawn by Koyama et al. (2013b).

We caution, however, that the dust extinction issue is still an important key question to fully assess the real environmental impacts on the SF main sequence. Indeed, we do find a marginal trend that the dust extinction effect ($A_{\rm H\alpha}$) is weakly correlated with local density in the sense that SF galaxies in higher-density environment tend to be more highly obscured by dust. A similar implication was obtained for $z = 0.4$ galaxies by Koyama et al. (2013b). In that work, we used SFR$_{\rm IR}$/SFR$_{\rm H\alpha}$ ratio (with 24 μm stacking analysis) to show that SF galaxies in high-density environments tend to be dustier (by $\sim$0.5 mag level) than those in under-dense environments, in qualitative agreement with the current work.

Our studies thus suggest a possibility that SF galaxies surviving in high-z cluster environments tend to be dustier, and perhaps the nature/mode of SF activity in cluster environments may be different from those in general field environments. We recall that the environmental impacts on the dust properties of galaxies are still very poorly understood at this moment, and there are some contradicting results on this issue (Garn et al. 2010; Patel et al. 2011). Therefore, special care must be taken on the dust extinction correction when we interpret the environmental dependence of the SF main sequence, and this key issue needs to be studied more in detail with larger galaxy samples in the future.

Finally, we comment on the possibility of the environmental impacts on the "scatter" of the SF main sequence. As we showed in Figure 12, we do not find a correlation between ΔMS and $\Sigma_{\rm 5th}$, consistent with the environmental independence of the location of the main sequence. On the other hand, we find a tentative hint that the ΔMS value more strongly deviates for those having a close companion within $\lesssim$200 kpc, while more isolated galaxies tend to be more steadily located on the SF main sequence. The sample is clearly too small to draw any firm conclusion, but this result may provide us with a new insight on the origin of the scatter of the SF main sequence. If a galaxy approaches another galaxy, their SF activity would be disturbed (some are boosted and others are truncated) due to the galaxy—galaxy interaction or halo gas stripping (satellite quenching). This would explain the larger scatter of the ΔMS for those with small $R_{\rm nearest}$, and the apparent environmental independence of the location of the SF main sequence.

7. SUMMARY AND CONCLUSIONS

We performed a broadband and narrow-band (Hα) imaging survey of a radio galaxy field (4C 65.22) at $z = 1.52$ over the $7' \times 4'$ FoV (corresponding to 3.6×2.0 Mpc^2) with MOIRCS/Suprime-Cam on the Subaru Telescope. Based on this new data set, we find a rich cluster candidate around the radio galaxy. We also studied an environmental dependence of galaxy properties around this newly discovered structure at $z \sim 1.5$. Our findings are summarized as follows.

1. With the photo-z and Hα emitter selections, we discovered a strong over-density of galaxies around 4C 65.22. We find that the cluster central region ($r \lesssim 250$ kpc from the density peak) is clearly dominated by passive red-sequence galaxies without Hα emission, while the Hα-emitting galaxies are preferentially located in the cluster outskirts, showing a sharp decline in the Hα emitter fraction toward the cluster center. This spatial segregation is similar to that seen in lower redshift clusters, suggesting that the newly discovered structure is a well-matured system.
2. The color–density and $M_\star$–density relations are already in place at $z \sim 1.5$. These environmental trends are mostly driven by passive red/massive galaxies residing in the cluster central region, whilst such environmental trends become much weaker when we consider only Hα emitters. This is also the case for SFR–density and SSFR–density relation. An excess of non-Hα-emitting red-sequence galaxies in the cluster core strongly suggests that the SF activity is suppressed in the very rich environment at $z = 1.5$, but the SF activity amongst SF galaxies are almost independent of environment.
3. There may exist a weak correlation between dust attenuation (derived with $\mathrm{SFR_{H\alpha}/SFR_{UV}}$ ratio) and local environment for SF galaxies at $z = 1.5$: galaxies in high-density environments tend to be dustier by $\sim$0.5–1.0 mag level. However, even if we take this point into account, we cannot see a detectable environmental variation in the location of the SF main sequence, consistent with recent studies. We do not find any correlation between the SFR offset from the SF main sequence (ΔMS) and $\Sigma_{5\mathrm{th}}$, but we find a tentative hint that galaxies having a close companion (at a moderate distance of $\lesssim$200 kpc) tend to be more largely scattered from the SF main sequence than more isolated galaxies.

The broadband and narrow-band imaging data used in this paper are collected at the Subaru Telescope, which is operated by the National Astronomical Observatory of Japan (NAOJ). We thank the referee for reviewing our paper and providing us with useful comments which improved the paper. Y.K., K.T., and M.H. acknowledge support from the Japan Society for the Promotion of Science (JSPS) through JSPS research fellowships for Young Scientists. This work was financially supported in part by a Grant-in-Aid for the Scientific Research (Nos. 21340045; 24244015) by the Japanese Ministry of Education, Culture, Sports and Science.

Facility: Subaru

REFERENCES

Alberts, S., Pope, A., Brodwin, M., et al. 2014, MNRAS, 437, 437
Balogh, M., Eke, V., Miller, C., et al. 2004, MNRAS, 348, 1355
Bassett, R., Papovich, C., Lotz, J. M., et al. 2013, ApJ, 770, 58
Bauer, A. E., Conselice, C. J., Pérez-González, P. G., et al. 2011a, MNRAS, 417, 289
Bauer, A. E., Grützbauch, R., Jørgensen, I., Varela, J., & Bergmann, M. 2011b, MNRAS, 411, 2009
Bertin, E., & Arnouts, S. 1996, A&AS, 117, 393
Best, P. N., Lehnert, M. D., Miley, G. K., & Röttgering, H. J. A. 2003, MNRAS, 343, 1
Böhringer, H., Voges, W., Huchra, J. P., et al. 2000, ApJS, 129, 435
Brammer, G. B., van Dokkum, P. G., & Coppi, P. 2008, ApJ, 686, 1503
Brinchmann, J., Charlot, S., White, S. D. M., et al. 2004, MNRAS, 351, 1151
Brinkmann, W., Chester, M., Kollgaard, R., et al. 1999, A&AS, 134, 221
Brodwin, M., Stanford, S. A., Gonzalez, A. H., et al. 2013, ApJ, 779, 138
Buat, V., Boselli, A., Gavazzi, G., & Bonfanti, C. 2002, A&A, 383, 801
Bunker, A. J., Warren, S. J., Hewett, P. C., & Clements, D. L. 1995, MNRAS, 273, 513
Calzetti, D., Armus, L., Bohlin, R. C., et al. 2000, ApJ, 533, 682
Cardelli, J. A., Clayton, G. C., & Mathis, J. S. 1989, ApJ, 345, 245
Chuter, R. W., Almaini, O., Hartley, W. G., et al. 2011, MNRAS, 413, 1678
Cooke, E. A., Hatch, N. A., Muldrew, S. I., Rigby, E. E., & Kurk, J. D. 2014, MNRAS, 440, 3262
Cooper, M. C., Coil, A. L., Gerke, B. F., et al. 2010, MNRAS, 409, 337
Cooper, M. C., Newman, J. A., Weiner, B. J., et al. 2008, MNRAS, 383, 1058
Cucciati, O., Iovino, A., Marinoni, C., et al. 2006, A&A, 458, 39
Daddi, E., Cimatti, A., Renzini, A., et al. 2004, ApJ, 617, 746
Daddi, E., Dickinson, M., Morrison, G., et al. 2007, ApJ, 670, 156
Dressler, A. 1980, ApJ, 236, 351
Elbaz, D., Daddi, E., Le Borgne, D., et al. 2007, A&A, 468, 33
Elbaz, D., Dickinson, M., Hwang, H. S., et al. 2011, A&A, 533, A119
Fassbender, R., Nastasi, A., Böhringer, H., et al. 2011, A&A, 527, L10
Galametz, A., Stern, D., Pentericci, L., et al. 2013, A&A, 559, A2
Galametz, A., Stern, D., Stanford, S. A., et al. 2010, A&A, 516, A101
Garn, T., & Best, P. N. 2010, MNRAS, 409, 421
Garn, T., Sobral, D., Best, P. N., et al. 2010, MNRAS, 402, 2017
Gobat, R., Daddi, E., Onodera, M., et al. 2011, A&A, 526, A133
Gómez, P. L., Nichol, R. C., Miller, C. J., et al. 2003, ApJ, 584, 210
Goto, T., Yamauchi, C., Fujita, Y., et al. 2003, MNRAS, 346, 601
Greene, C. R., Gilbank, D. G., Balogh, M. L., et al. 2012, MNRAS, 425, 1738
Grützbauch, R., Bauer, A. E., Jørgensen, I., & Varela, J. 2012, MNRAS, 423, 3652
Grützbauch, R., Conselice, C. J., Bauer, A. E., et al. 2011, MNRAS, 418, 938
Gunn, J. E., & Stryker, L. L. 1983, ApJS, 52, 121
Hayashi, M., Kodama, T., Koyama, Y., et al. 2010, MNRAS, 402, 1980
Hayashi, M., Kodama, T., Koyama, Y., et al. 2014, MNRAS, 439, 2571
Hayashi, M., Kodama, T., Koyama, Y., Tadaki, K.-I., & Tanaka, I. 2011, MNRAS, 415, 2670
Hayashi, M., Kodama, T., Tadaki, K.-i., Koyama, Y., & Tanaka, I. 2012, ApJ, 757, 15
Hatch, N. A., Kurk, J. D., Pentericci, L., et al. 2011, MNRAS, 415, 2993
Hilton, M., Lloyd-Davies, E., Stanford, S. A., et al. 2010, ApJ, 718, 133
Hwang, H. S., Elbaz, D., Dickinson, M., et al. 2011, A&A, 535, A60
Ibar, E., Sobral, D., Best, P. N., et al. 2013, MNRAS, 434, 3218
Ichikawa, T., Suzuki, R., Tokoku, C., et al. 2006, Proc. SPIE, 6269, 38
Ideue, Y., Nagao, T., Taniguchi, Y., et al. 2009, ApJ, 700, 971
Iye, M., Karoji, H., Ando, H., et al. 2004, PASJ, 56, 381
Kajisawa, M., Ichikawa, T., Yamada, T., et al. 2010, ApJ, 723, 129
Kajisawa, M., Kodama, T., Tanaka, I., Yamada, T., & Bower, R. 2006, MNRAS, 371, 577
Kashino, D., Silverman, J. D., Rodighiero, G., et al. 2013, ApJL, 777, L8
Kennicutt, R. C., Jr. 1998, ARA&A, 36, 189
Kennicutt, R. C., Jr., & Kent, S. M. 1983, AJ, 88, 1094
Kinney, A. L., Calzetti, D., Bohlin, R. C., et al. 1996, ApJ, 467, 38
Kodama, T., Arimoto, N., Barger, A. J., & Arag'on-Salamanca, A. 1998, A&A, 334, 99
Kodama, T., Balogh, M. L., Smail, I., Bower, R. G., & Nakata, F. 2004, MNRAS, 354, 1103
Kodama, T., Hayashi, M., Koyama, Y., et al. 2013, in IAU Symp. 295, The Intriguing Life of Massive Galaxies, ed. D. Thomas, H. Pasquali, & I. Ferreras (Cambridge: Cambridge Univ. Press), 74
Kodama, T., Smail, I., Nakata, F., Okamura, S., & Bower, R. G. 2001, ApJL, 562, L9
Kodama, T., Tanaka, I., Kajisawa, M., et al. 2007, MNRAS, 377, 1717
Kollgaard, R. I., Brinkmann, W., Chester, M. M., et al. 1994, ApJS, 93, 145
Kollgaard, R. I., Feigelson, E. D., Laurent-Muehleisen, S. A., et al. 1995, ApJ, 449, 61
Koyama, Y., Kodama, T., Nakata, F., Shimasaku, K., & Okamura, S. 2011, ApJ, 734, 66
Koyama, Y., Kodama, T., Shimasaku, K., et al. 2010, MNRAS, 403, 1611

Koyama, Y., Kodama, T., Tadaki, K.-i., et al. 2013b, MNRAS, 428, 1551
Koyama, Y., Kodama, T., Tanaka, M., Shimasaku, K., & Okamura, S. 2007, MNRAS, 382, 1719
Koyama, Y., Smail, I., Kurk, J., et al. 2013a, MNRAS, 434, 423
Kurk, J., Cimatti, A., Zamorani, G., et al. 2009, A&A, 504, 331
Kurk, J. D., Pentericci, L., Röttgering, H. J. A., & Miley, G. K. 2004, A&A, 428, 793
Kurk, J. D., Röttgering, H. J. A., Pentericci, L., et al. 2000, A&A, 358, L1
Lacy, M., Hill, G. J., Kaiser, M.-E., & Rawlings, S. 1993, MNRAS, 263, 707
Lawrence, A., Warren, S. J., Almaini, O., et al. 2007, MNRAS, 379, 1599
Lewis, I., Balogh, M., De Propris, R., et al. 2002, MNRAS, 334, 673
Li, I. H., Glazebrook, K., Gilbank, D., et al. 2011, MNRAS, 411, 1869
Lidman, C., Rosati, P., Tanaka, M., et al. 2008, A&A, 489, 981
Lin, L., Jian, H.-Y., Foucaud, S., et al. 2014, ApJ, 782, 33
Matsuda, Y., Smail, I., Geach, J. E., et al. 2011, MNRAS, 416, 2041
Madau, P., Ferguson, H. C., Dickinson, M. E., et al. 1996, MNRAS, 283, 1388
McGee, S. L., Balogh, M. L., Wilman, D. J., et al. 2011, MNRAS, 413, 996
Miyazaki, S., Komiyama, Y., Sekiguchi, M., et al. 2002, PASJ, 54, 833
Muzzin, A., Wilson, G., Demarco, R., et al. 2013, ApJ, 767, 39
Muzzin, A., Wilson, G., Yee, H. K. C., et al. 2012, ApJ, 746, 188
Nastasi, A., Fassbender, R., Böhringer, H., et al. 2011, A&A, 532, L6
Newman, A. B., Ellis, R. S., Andreon, S., et al. 2014, ApJ, 788, 51
Noeske, K. G., Weiner, B. J., Faber, S. M., et al. 2007, ApJL, 660, L43
Ouchi, M., Shimasaku, K., Okamura, S., et al. 2004, ApJ, 611, 660
Papovich, C., Momcheva, I., Willmer, C. N. A., et al. 2010, ApJ, 716, 1503
Park, C., & Hwang, H. S. 2009, ApJ, 699, 1595
Patel, S. G., Kelson, D. D., Holden, B. P., Franx, M., & Illingworth, G. D. 2011, ApJ, 735, 53
Peng, Y.-j., Lilly, S. J., Kovač, K., et al. 2010, ApJ, 721, 193
Peng, Y.-j., Lilly, S. J., Renzini, A., & Carollo, M. 2012, ApJ, 757, 4
Price, S. H., Kriek, M., Brammer, G. B., et al. 2013, arXiv:1310.4177
Quadri, R. F., Williams, R. J., Franx, M., & Hildebrandt, H. 2012, ApJ, 744, 88
Rodighiero, G., Cimatti, A., Gruppioni, C., et al. 2010, A&A, 518, L25
Saintonge, A., Tacconi, L. J., Fabello, S., et al. 2012, ApJ, 758, 73
Salpeter, E. E. 1955, ApJ, 121, 161
Santini, P., Fontana, A., Grazian, A., et al. 2009, A&A, 504, 751
Santos, J. S., Altieri, B., Popesso, P., et al. 2013, MNRAS, 433, 1287
Santos, J. S., Fassbender, R., Nastasi, A., et al. 2011, A&A, 531, L15
Schlegel, D. J., Finkbeiner, D. P., & Davis, M. 1998, ApJ, 500, 525
Scoville, N., Arnouts, S., Aussel, H., et al. 2013, ApJS, 206, 3
Shimakawa, R., Kodama, T., Tadaki, K.-I., et al. 2014, MNRAS, 441, L1
Smail, I., Geach, J. E., Swinbank, A. M., et al. 2014, ApJ, 782, 19
Sobral, D., Best, P. N., Matsuda, Y., et al. 2012, MNRAS, 420, 1926
Sobral, D., Best, P. N., Smail, I., et al. 2011, MNRAS, 411, 675
Sobral, D., Smail, I., Best, P. N., et al. 2013, MNRAS, 428, 1128
Stanford, S. A., Brodwin, M., Gonzalez, A. H., et al. 2012, ApJ, 753, 164
Steidel, C. C., Adelberger, K. L., Shapley, A. E., et al. 2005, ApJ, 626, 44
Stott, J. P., Smail, I., Edge, A. C., et al. 2007, ApJ, 661, 95
Suzuki, R., Tokoku, C., Ichikawa, T., et al. 2008, PASJ, 60, 1347
Tacconi, L. J., Neri, R., Genzel, R., et al. 2013, ApJ, 768, 74
Tanaka, I., Breuck, C. D., Kurk, J. D., et al. 2011, PASJ, 63, 415
Tanaka, M., Finoguenov, A., Mirkazemi, M., et al. 2013, PASJ, 65, 17
Tanaka, M., Finoguenov, A., & Ueda, Y. 2010, ApJL, 716, L152
Tanaka, M., Goto, T., Okamura, S., Shimasaku, K., & Brinkmann, J. 2004, AJ, 128, 2677
Tadaki, K. I., Kodama, T., Koyama, Y., et al. 2011, PASJ, 63, 437
Tadaki, K. I., Kodama, T., Ota, K., et al. 2012, MNRAS, 423, 2617
Tadaki, K. I., Kodama, T., Tanaka, I., et al. 2013, ApJ, 778, 114
Tran, K.-V. H., Papovich, C., Saintonge, A., et al. 2010, ApJL, 719, L126
Venemans, B. P., Kurk, J. D., Miley, G. K., et al. 2002, ApJL, 569, L11
Venemans, B. P., Röttgering, H. J. A., Miley, G. K., et al. 2007, A&A, 461, 823
Villar, V., Gallego, J., Pérez-González, P. G., et al. 2008, ApJ, 677, 169
Vulcani, B., Poggianti, B. M., Finn, R. A., et al. 2010, ApJL, 710, L1
Whitaker, K. E., van Dokkum, P. G., Brammer, G., & Franx, M. 2012, ApJL, 754, L29
Wijesinghe, D. B., Hopkins, A. M., Brough, S., et al. 2012, MNRAS, 423, 3679
Wuyts, S., Förster Schreiber, N. M., Nelson, E. J., et al. 2013, ApJ, 779, 135
Wuyts, S., Förster Schreiber, N. M., van der Wel, A., et al. 2011, ApJ, 742, 96
Yagi, M., Kashikawa, N., Sekiguchi, M., et al. 2002, AJ, 123, 66
Zeimann, G. R., Stanford, S. A., Brodwin, M., et al. 2013, ApJ, 779, 137
Ziparo, F., Popesso, P., Finoguenov, A., et al. 2013, MNRAS, 434, 3089
Ziparo, F., Popesso, P., Finoguenov, A., et al. 2014, MNRAS, 437, 458